Distributions of total and size-fractionated particulate ^{210}Po and ^{210}Pb activities along the North Atlantic GEOTRACES GA01 (GEOVIDE) transect

Yi Tang[1,2], Maxi Castrillejo[3,4], Montserrat Roca-Martí[3], Pere Masqué[3,5], Nolwenn Lemaitre[6], Gillian Stewart[2,1]

[1] Earth and Environmental Sciences, the Graduate Center, City University of New York, New York, USA

[2] School of Earth and Environmental Sciences, Queens College, City University of New York, Flushing, USA

[3] Institut de Ciència i Tecnologia Ambientals & Departament de Física, Universitat Autònoma de Barcelona, Bellaterra, 08193, Spain

[4] Laboratory of Ion Beam Physics, ETH-Zürich, Otto-Stern-Weg 5, Zürich, 8093, Switzerland

[5] School of Science and Centre for Marine Ecosystems Research, Edith Cowan University, Joondalup, Western Australia, Australia

[6] Department of Earth Sciences, Institute of Geochemistry and Petrology, ETH-Zürich, Zürich, Switzerland

Correspondence to: Gillian Stewart (Gillian.Stewart@qc.cuny.edu)

Abstract

Vertical distributions of total and particulate ^{210}Po and ^{210}Pb activities in the water column were measured at eleven stations in the North Atlantic during the GEOTRACES GA01 GEOVIDE cruise in May - June 2014. Total ^{210}Po activity was on average 24% lower than ^{210}Pb activity in the upper 100 m, and was closer to unity in the mesopelagic (100 – 1000 m). The partitioning coefficients (K_d) along the transect suggest the preferential association of ^{210}Po relative to ^{210}Pb onto particles. The prominent role of small particles in sorption was confirmed by the observation that over 80% of the particulate radionuclide activity was on small particles. To account for the observed surface water ^{210}Po/^{210}Pb disequilibria, particulate radionuclide activities and export of both small (1-53 μm) and large (> 53 μm) particles must be considered. A comparison between the GEOVIDE total particulate ^{210}Po/^{210}Pb activity ratios (AR) and the ratios in previous studies revealed a distinct geographic distribution, with lower particulate AR in the high-latitude North Atlantic (including this study) and Arctic in relation to all other samples. For the samples where apparent oxygen utilization (AOU) was calculated at the same depth and time as the ^{210}Po/^{210}Pb AR (40 stations including this study), there was a two-phase correlation between the total particulate AR and AOU likely reflecting the nature of the particles and demonstrating the forces of remineralization and radionuclide decay from particles as they age.

1 Introduction

The major goal of the international GEOTRACES program is to characterize the distributions of trace elements and isotopes (TEIs) in the ocean on a global scale, and to identify and quantify processes that control these distributions (GEOTRACES Planning Group, 2006). The GEOVIDE section was a contribution of the French GEOTRACES program to this global program in the subpolar North Atlantic. The GEOVIDE GA01 cruise was carried out in 2014 in the North Atlantic and consisted of two sections: a section along the OVIDE (Observatoire de la variabilité interannuelle et décennale en Atlantique Nord) line between Lisbon (Portugal) and Cape Farewell (southern tip of Greenland), and a Cape Farewell to St. John's (Canada) section across the Labrador Sea (Fig. 1). Since 2002, the OVIDE section has been occupied biennially to collect physical and biogeochemical data (Mercier et al., 2015). The knowledge of the currents, water masses, and biogeochemical provinces gained from the previous OVIDE campaigns enabled the optimal strategy for TEIs sampling and provided help for the interpretation of the distribution of TEIs in the subpolar North Atlantic (García-Ibáñez et al., 2015). In addition to the OVIDE line, the Labrador Sea section provided a unique opportunity to study TEIs distributions along the boundary current of the western North Atlantic subpolar gyre (Sarthou et al., in review).

Polonium-210 (^{210}Po, $T_{1/2}$ = 138.4 d) and its radioactive grandparent Lead-210 (^{210}Pb, $T_{1/2}$ = 22.3 y) are two non-conservative ^{238}U decay series products. The GEOTRACES program has included both radionuclides in its TEIs list primarily due to ^{210}Po's enhanced bioaccumulation and the use of the ^{210}Po/^{210}Pb pair as a proxy for assessing particle export in the upper ocean. The distribution of ^{210}Po and ^{210}Pb has been widely measured over the last several decades in the Atlantic (e.g. Bacon et al., 1976; Sarin et al., 1999; Rigaud et al., 2015; Ceballos-Romero et al., 2016), Pacific (e.g. Nozaki and Tsunogai, 1976; Murray et al., 2005; Verdeny et al., 2008), Indian (e.g. Cochran et al., 1983; Sarin et al., 1994; Subha Anand et al., 2017), Arctic (e.g. Moore and Smith, 1986; He et al., 2015; Roca-Martí et al., 2016) and Southern Oceans (e.g. Shimmield et al., 1995; Friedrich and Rutgers van der Loeff, 2002). However, since the data reported by Bacon et al., (1980b) at the Labrador Sea stations (47.8 – 53.7 °N), there are few studies of ^{210}Po and ^{210}Pb activity in the North Atlantic at latitudes greater than 40 °N. The GEOVIDE cruise, which targeted the North Atlantic from 40 °N to 60 °N, provided an opportunity to fill this data gap.

Besides ascertaining the distribution of the natural radionuclides under specific geographic conditions, this project aimed to answer questions about their biogeochemical behaviors in various

marine environments. Owing to the significantly longer half-life of ^{210}Pb relative to ^{210}Po, the two radionuclides are expected to be in secular equilibrium (total ^{210}Po/^{210}Pb activity ratio = 1) in the ocean, assuming no net removal or addition of either radionuclide. A deficit of ^{210}Po activity relative to ^{210}Pb activity (^{210}Po/^{210}Pb activity ratio < 1), however, is commonly found in the upper ocean (e.g. Bacon et al., 1976; Nozaki and Tsunogai, 1976; Cochran et al., 1983; Sarin et al., 1999). This has been attributed to a higher particle reactivity of ^{210}Po (higher partitioning coefficient, K_d) than ^{210}Pb in seawater. Particles, therefore, become enriched in ^{210}Po (^{210}Po/^{210}Pb activity ratio > 1) and their sinking to deeper waters results in a ^{210}Po activity deficit relative to ^{210}Pb activity in the upper water column where particles are formed.

In this work, we describe the distributions of total and size-fractionated particulate ^{210}Po and ^{210}Pb activity along the GEOVIDE cruise in the North Atlantic. These data are a significant contribution to the high-latitude North Atlantic ^{210}Po and ^{210}Pb activity data set. We present a compilation of particulate ^{210}Po/^{210}Pb activity ratios (AR) from previous studies in the global ocean and the results are discussed in regards to the aging of water and biochemical processes. We also describe the relationship among small particles, adsorption, and scavenging of radionuclides. These results lead to recommendations for the estimation of particulate organic carbon export flux based on the ^{210}Po/^{210}Pb disequilibrium, a topic that is covered in a companion paper (Tang et al., , companion paper submitted to this volume).

2 Methods

2.1 Sample collection

The French GEOTRACES cruise to the North Atlantic (GEOVIDE, Section GA01; May 15 – June 30, 2014) was completed on the *R/V Pourquoi Pas?*. The research vessel departed from Lisbon, Portugal, headed northwest to the Greenland shelf, crossed the Labrador Sea, and ended in St John's, Newfoundland, Canada (Fig. 1). A rosette equipped with conductivity-temperature-depth sensors and 12 L Niskin bottles was used to collect 200 seawater samples (5 – 10 L each) from 10 full water column "super" (10 multi-cast) stations (16 – 22 depths/station) and 1 "XLarge" (5-cast) station to 800 m (station 26, 9 depths) for the determination of total ^{210}Po and ^{210}Pb activity. Upon recovery, seawater samples were transferred to 10 L acid-cleaned containers. In addition, particulate radionuclide activities in two size classes (1-53 µm and > 53 µm) were collected at 3 – 10 depths per station using large volume *in-situ* filtration systems (Challenger Oceanic pumps and

McLane pumps) equipped with 142 mm filter holders. Each filter head contained a stacked 53 μm PETEX screen followed by a 1 μm pore size quartz fiber QMA filter. The volume filtered was determined via flow meters mounted below each filter head, and the mean volume pumped through each head was 881 L. Once recovered, clear polyethylene caps were placed on the top of the pump heads and they were brought into a clean laboratory for sub-sampling.

2.2 Total ^{210}Po and ^{210}Pb

Total ^{210}Po and ^{210}Pb activities were determined from the seawater samples by the cobalt-ammonium pyrrolidine dithiocarbamate (Co-APDC) technique (Fleer and Bacon, 1984). Samples were acidified to a pH < 2 with concentrated HCl immediately after collection and spiked with known amounts of ^{209}Po and stable lead as chemical yield tracers. After vigorous stirring and at least 12 h of isotope equilibration, cobalt nitrate and APDC solutions were added to co-precipitate Po and Pb. Samples were filtered through a 0.45 μm membrane filter and the filters with the precipitate were placed into clean falcon tubes, sealed with parafilm, and stored in double-bags. As the delay between sample collection and first Po plating increases, the uncertainty of the calculated ^{210}Po activity also increases. In addition, it is necessary to balance counting periods with the number of samples as the uncertainty due to alpha spectrometry counting decreases by increasing the counting time. To limit the delay between sampling and processing and to ensure higher counting statistics by having more alpha spectrometers devoted to this project, sample processing and analyses were split between Universitat Autònoma de Barcelona (UAB) (samples from stations 1, 13, and 21) and Queens College (QC) (stations 26, 32, 38, 44, 60, 69, and 77). Both laboratories followed the same procedure. Briefly, the filters were digested into a solution of concentrated HNO_3 and HCl, and after the solution was evaporated to dryness, the samples were recovered in 1M and 0.5 M HCl solution at UAB and QC, respectively (a 0.5-2 M HCl solution is recommended, Rigaud et al., 2013). A polished pure silver disc (Flynn, 1968) with one side covered by enamel paint was placed into the weak acid solution and heated so that the polonium nuclides were spontaneously plated onto only one side of the disc. The activities of both Po nuclides on the disc were measured by alpha spectrometry. Any ^{210}Po and ^{209}Po remaining in the plating solution was removed using AG 1-X8 anion exchange resin and the final solution was re-spiked with ^{209}Po and stored for more than 6 months to allow ingrowth of ^{210}Po from the decay of ^{210}Pb.

The ^{210}Pb activity was then determined by re-plating the solutions using silver discs and measuring the ingrown ^{210}Po. Two aliquots of the plating solutions for each sample were taken before the first and second platings for the measurement of total Pb concentration by inductively coupled plasma mass spectrometry (ICP-MS) to determine sample recovery during processing. The average recoveries produced by UAB and QC were 83 ± 11% (n = 54) and 76 ± 14% (n = 144), respectively. The activities of ^{210}Po and ^{210}Pb at the time of collection were determined by a series of corrections, including nuclide decay, ingrowth, chemical recoveries, detector backgrounds, and blank contamination following the methods in Rigaud et al., (2013). The activity uncertainties from UAB were on average 8% for both ^{210}Po and ^{210}Pb activity, while the QC uncertainties were on average 13% for ^{210}Po activity and 16% for ^{210}Pb activity. The greater uncertainties of ^{210}Po and ^{210}Pb activities in the samples processed at QC were due to the longer delay between sampling and first plating (68 vs. 50 d) and higher uncertainties in the determination of the recovery of lead.

2.3 Particulate ^{210}Po and ^{210}Pb

After collection via in situ pumping, one quarter (equivalent to ~ 220 L) of the PETEX screen containing > 53 μm or "large" particles was processed for radionuclide activity. Swimmers were carefully removed from all samples. The QMA filters containing 1-53 μm or "small" particles were sub-sampled (2 – 4 punches of 12 mm-diameter) achieving a mean effective volume of ~ 66 L. The screens and punches were stored in double-bags at -80 °C until the analyses onshore. The particulate samples were split between the two laboratories in parallel to the seawater samples. The filters were spiked with ^{209}Po tracer solution and stable lead, digested using a mixture of concentrated HF, HNO_3 and HCl at UAB, but only HNO_3 and HCl at QC. After multiple rounds of digestion and evaporation to near dryness, the samples were recovered in 0.5 M HCl solution. Any remaining pieces of filter which were not completely digested were carefully removed, rinsed with 0.5 M HCl solution several times, and then discarded. The analyses of the particulate radionuclide activities were identical to those for the seawater samples described in section 2.2.

2.4 Concentration of suspended particulate matter (SPM)

The Helene Planquette group (University of Brest, co-authors in this issue) collected subsamples from the same screens and filters that were sampled previously for radionuclides to

159 determine major phase composition (particulate organic matter (POM), lithogenic material,
160 calcium carbonate ($CaCO_3$), opal, $Fe(OH)_3$, and MnO_2) (references therein Lam et al., 2015). The
161 mass concentration of SPM was calculated as the sum of the chemical dry weight of the major
162 particulate phases.
163 The calculated SPM concentration was compared to the *in-situ* transmission data obtained from
164 the rosette CTD sensor (Fig. S1). The overall negative relationship was statistically significant (R^2
165 = 0.7, n = 53, $p < 0.0001$), suggesting that the SPM concentrations determined were reasonable
166 estimates of particle concentration in the water column. We used the SPM values to determine the
167 partitioning coefficient, K_d, for ^{210}Po and ^{210}Pb in section 4.4.
168
169 **2.5 Satellite-based data**
170 The 8-day composites of surface chlorophyll-a concentration for each station were retrieved
171 from NASA's MODIS products (https://oceancolor.gsfc.nasa.gov) for the period from January to
172 July 2014. The time-series chlorophyll-a concentrations were used to show the development of a
173 phytoplankton bloom over time along the transect.
174
175 **2.6 Historical values**
176 The historical data of the particulate ^{210}Po and ^{210}Pb activity, and the hydrological parameters
177 (pressure, temperature, salinity, and dissolved oxygen) were obtained from databases and
178 publications. The location, date, database address or publication name, and type of data (particulate
179 ^{210}Po and ^{210}Pb activity or hydrological parameters) from all other studies is listed in supplemental
180 Table S1.
181
182 **2.7 Apparent oxygen utilization**
183 Apparent oxygen utilization ($AOU = O_{2\,saturated} - O_{2\,measured}$) is defined as the difference between
184 the saturated oxygen at a given temperature and salinity and the measured in-situ oxygen
185 concentration (Ito et al., 2004; Duteil et al., 2013). A positive AOU indicates either water mass
186 aging and outgassing of oxygen or biological activity, namely respiration (e.g. Keeling et al., 1998;
187 Boyer et al., 1999). Negative AOU, indicating that the water is oversaturated with dissolved
188 oxygen, can appear under the conditions of an intense bloom (e.g. Coppola et al., 2017).

The dissolved oxygen concentration was measured by Winkler titration and the saturated oxygen concentration was calculated as a function of in-situ temperature and salinity, and one atmosphere of total pressure based on the built-in function in Ocean Data View (https://odv.awi.de).

2.8 Statistical analyses

Statistical analyses were carried out in R Studio version 3 using Fitting Linear Models, and Welch Two Sample t-tests. Linear regression analysis was used to investigate the relationship between total particulate $^{210}Po/^{210}Pb$ AR and AOU. The Welch Two Sample t-test was applied to assess whether the mean of the total particulate $^{210}Po/^{210}Pb$ AR was the same as the mean of the small particulate $^{210}Po/^{210}Pb$ AR. It was also applied to investigate the means of the total ^{210}Pb activity in the western and eastern sections along the transect.

3 Results

3.1 Total ^{210}Po and ^{210}Pb activities

Total ^{210}Po activities ($^{210}Po_t$) in all samples ranged from 2.2 to 16.4 dpm 100 L^{-1} and the mean $^{210}Po_t$ was 8.8 ± 2.4 dpm 100 L^{-1} (n = 198, Fig. 2). $^{210}Po_t$ activities were generally low within the mixed layer and euphotic zone (15 – 47 m), slightly increased or remained relatively constant in the depth range between the mixed layer and 250 m, and then decreased with water depth at most of the stations except station 26. Near the seafloor, stations 1, 13 and 44 had a slight increase of $^{210}Po_t$ activity.

Total ^{210}Pb activities ($^{210}Pb_t$) were between 2.1 and 20.6 dpm 100L^{-1} with a mean value of 10.0 ± 3.0 dpm 100 L^{-1} (n = 198, Fig. 2). $^{210}Pb_t$ activities were low in the surface, slightly increased in the subsurface and decreased with water depth. Stations 1, 13, 44, and 60 exhibited an increase near the seafloor.

The mean $^{210}Po_t/^{210}Pb_t$ activity ratio (AR) of all samples was 0.92 ± 0.28 (n = 198, Fig. 2). When considering different basins separately, there is a tendency of decreasing $^{210}Po_t/^{210}Pb_t$ AR from the West European Basin (1.10 ± 0.35) westwards to the Iceland Basin (0.90 ± 0.19) and the Irminger Sea and the Labrador Sea (0.80 ± 0.18 and 0.83 ± 0.21, respectively).

For all regions, significant deficits of $^{210}Po_t$ (0.80 ± 0.20, n = 40) were observed within the mixed layer and euphotic zone (Fig. 3). Secular equilibrium was also observed at some shallow depths (i.e. 80 m at station 44) and even in surface waters (i.e. 15 m at station 38). $^{210}Po_t$ excesses

relative to $^{210}Pb_t$, which were larger than $^{210}Po_t$ surface depletions at the same stations, were observed below the surface at some depths at stations 1, 13, and 21 in the West European Basin (Fig. 2). At depths below the surface to ~ 1500 m in the Iceland Basin, the Irminger Sea, and the Labrador Sea, the water samples still indicated a ^{210}Po deficiency (AR: 0.84 ± 0.17, n = 27). Secular equilibrium was generally reached near the bottom depths in all basins except at stations 13 and 60 where the water samples were either enriched in $^{210}Po_t$ ($^{210}Po_t/^{210}Pb_t$ AR = 1.58 ± 0.16) or depleted in $^{210}Po_t$ ($^{210}Po_t/^{210}Pb_t$ AR = 0.50 ± 0.12), respectively.

3.2 Particulate ^{210}Po and ^{210}Pb activities

Small particulate ^{210}Po ($^{210}Po_s$) activities varied in a wide range from 0.08 to 4.82 dpm $100L^{-1}$ (mean: 0.76 ± 0.63 dpm $100L^{-1}$, n = 81), about 83% of the values in the small particles were lower than 1.0 dpm $100L^{-1}$ with higher $^{210}Po_s$ values generally observed in the surface samples (Fig. 4, Table S2). The range of small particulate ^{210}Pb ($^{210}Pb_s$) activities was 0.07 to 2.89 dpm $100L^{-1}$ (mean: 0.56 ± 0.46 dpm $100L^{-1}$, n = 81). The vertical profiles of $^{210}Pb_s$ were generally similar to those of $^{210}Po_s$, with relatively high activity in the surface, lower activity in the subsurface and increasing activity with depth (Fig. 4). This has been seen in the North Atlantic along the GEOTRACES GA03 transect (Rigaud et al., 2015). The mean $^{210}Po_s/^{210}Pb_s$ activity ratio (AR) was 1.43 ± 0.96 in the surface waters (n = 14, ≤ 47 m), and 1.57 ± 0.90 with all samples included (n = 81, 8 – 3440 m). While most surface observations had an AR of $^{210}Po_s/^{210}Pb_s$ higher than unity, 5 surface samples at stations 69 and 77 showed an enrichment of ^{210}Pb activity over ^{210}Po ($^{210}Po_s/^{210}Pb_s$ AR: 0.62 ± 0.18).

Large particulate ^{210}Po ($^{210}Po_l$) activities ranged from 0.01 to 0.83 dpm $100L^{-1}$ with a mean of 0.10 ± 0.12 dpm $100L^{-1}$ (n = 59, Fig. 5, Table S2). The range of ^{210}Pb activity in the large particles ($^{210}Pb_l$) was from 0.02 to 0.67 dpm $100L^{-1}$ (mean: 0.12 ± 0.14 dpm $100L^{-1}$, n = 59). The highest $^{210}Po_l$ and $^{210}Pb_l$ values were found at 30 m at station 26. The mean $^{210}Po_l/^{210}Pb_l$ activity ratio (AR) was 1.09 ± 1.54 in the surface waters (n = 14, ≤ 47 m), and 1.06 ± 0.86 when all data were considered (n = 59, 8-800 m). There were 17% of the samples with a depletion of ^{210}Po activity relative to ^{210}Pb activity in large particles (mean AR: 0.49 ± 0.23), particularly in surface waters from the western section. We address this issue further in sections 4.2 and 4.3.

The percentages of total ^{210}Po activity in the small and large particles ranged from 0.9 to 46.7% (mean: 8.0 ± 6.7%) and from 0.1 to 8.9% (mean: 1.2 ± 1.5%), respectively. The percentage of total

^{210}Pb activity ranged from 0.7 to 21.4% (mean: 4.9 ± 3.8%) and from 0.2 to 5.9% (mean: 1.1 ± 1.2%) in the small and large particulate phase, respectively. These values revealed that both radionuclides were predominantly present in the dissolved phase along this transect, as is commonly found in the ocean. The particulate percentages reported here are similar to the values reported from the F.S. "Meteor" cruise 32 in the North Atlantic (Bacon et al., 1976) and along the North Atlantic GA03 transect (Rigaud et al., 2015).

We then combined radionuclide activity on the small and large particles from the same depth as the total particulate activity. There were 56 samples in total (surface to 800 m) and 41 of them were from the upper 200 m. Most of the total particulate ^{210}Po ($^{210}Po_p$) and ^{210}Pb ($^{210}Pb_p$) activity was on the small particles, with 86% of $^{210}Po_p$ and 80% of $^{210}Pb_p$ on the small size fraction (data not shown). The total particulate ^{210}Po and ^{210}Pb AR ($^{210}Po_p/^{210}Pb_p$) had the same mean as that of the small particulate ^{210}Po and ^{210}Pb AR ($^{210}Po_s/^{210}Pb_s$) (Welch Two Sample t-test, n = 56, $p = 0.1$), indicating that the values of the $^{210}Po_p/^{210}Pb_p$ activity ratios were driven by the small particles. While the majority of particulate matter was enriched in ^{210}Po ($^{210}Po_p/^{210}Pb_p$ AR> 1), there were 13 out of 56 total samples from various depths that were depleted in ^{210}Po relative to ^{210}Pb. The $^{210}Po_p/^{210}Pb_p$ activity ratios from this study are compared to the results from previous studies in various oceanic regimes in section 4.2.

4 Discussion

4.1 Total ^{210}Po and ^{210}Pb activities

The overall profiles of $^{210}Po_t$ and $^{210}Pb_t$ activities were different among basins (Fig. 2). The deficiencies of $^{210}Po_t$ activities with respect to $^{210}Pb_t$ activities in the surface samples from the Iceland Basin, the Irminger Sea, and the Labrador Sea were generally greater than those from the West European Basin. Such disequilibria generally extended to the deep waters (1700 – 2950 m). In contrast, $^{210}Po_t$ activities in the West European Basin were generally enriched relative to $^{210}Pb_t$ activities from below the surface to the bottom of the profile. In the West European Basin, the sub-surface $^{210}Po_t$ activity excess was much larger than the surface depletion, suggesting that some external source would be needed to maintain this excess ^{210}Po activity within the water column. One possible source of these sub-surface ^{210}Po activity excesses below 2000 m at stations 1 and 13 could be the North-East Atlantic Deep Water, lower ($NEADW_L$) which was the dominant water mass in the Iberian Basin from 2000 m to the bottom, and had a concentration of silicate up to 48

μmol kg^{-1} (García-Ibáñez et al., 2015). High activity of ^{210}Po in deep samples could be due to the dissolution of diatoms or herbivore feces (Cooper, 1952). As these particles sink and dissolve, ^{210}Po activity may have been preferentially released to the dissolved phase compared to ^{210}Pb activity (Bacon et al., 1976), leading to ^{210}Po excess observed in the deep waters at stations 1 and 13. For the sub-surface ^{210}Po activity excesses at station 1 between 400 and 1000 m where lateral inputs of particulate Fe from the margin was observed (Gourain et al., 2018), the likely process is diffusion of ^{210}Po from those particles originated from the margin and such excess could be transported westwards to station 13 by lateral advection. An alternative source of ^{210}Po activity excess between 50 and 250 m at stations 1 and 13 (Fig. 3) could be the eastern boundary upwelling along the coast of the Iberian Peninsula (García-Ibáñez et al., 2015). Even though no strong upwelling events were revealed from temperature and density profiles during the cruise, northerly winds favoring upwelling were recorded 2 – 3 months before the sampling (Shelley et al., 2017). The deep water may have excess ^{210}Po activity due to the remineralization of sinking particles. The upwelling of this water mass prior to the sampling date could maintain such sub-surface excess ^{210}Po activity. Similar findings have been reported in the Cariaco Trench for the upper 300 m of the water column by Bacon et al., (1980a).

As atmospheric deposition is the main source of ^{210}Pb to the water column (e.g. Masqué et al., 2002), we divided the GA01 transect into a western section (stn. 44 – 77) and an eastern section (stn. 1 – 38) based on atmospheric deposition boxes described in Shelley et al., (2017). Total atmospheric deposition fluxes of a suite of aerosol-sourced trace metals (TEs) were reported to be higher in the east than the west for 18 out of 19 TEs (Shelley et al., 2017). However, a two sample t-test revealed a greater mean of $^{210}Pb_t$ activity in surface waters in the western than in the eastern section ($p < 0.02$, mean: 12.1 vs. 10.4 dpm 100 L^{-1}), despite the fact that ^{210}Pb is usually associated with aerosols. Even though the direct input of atmospheric ^{210}Pb may be larger in the east (assuming it behaves like the other trace metals, but without aerosol ^{210}Pb data we cannot confirm this), alternative inputs of ^{210}Pb from freshwater (e.g., sea ice processes and meteoric water) could be a greater source of ^{210}Pb activity to the west. The freshwater sources over the Greenland shelf and slope have been identified by Benetti et al., (2017), and were believed to be an important source of Fe (Tonnard et al., in review) and Al (Menzel-Barraqueta et al., in review) off of Greenland during this cruise. This result highlights the need in the future to measure ^{210}Pb activity

simultaneously in the atmospheric and local freshwater sources in order to account for all source terms.

4.2 Total particulate $^{210}Po/^{210}Pb$ AR

A proposed explanation for the depletion of ^{210}Po activity relative to ^{210}Pb activity (AR <1) in some particles is effective recycling, commonly characterized by a subsurface excess of dissolved ^{210}Po activity released from enriched particles leaving the surface. Bacon et al., (1976) suggested that the efficiency of this recycling could reach up to 50%, while there is no significant concurrent release of ^{210}Pb activity in the water column. Laboratory studies have found the release rate of ^{210}Po in marine particulate matter to be significant; for example, 41% of the ^{210}Po activity in euphausiid fecal pellets was released over 5 days as presented in Heyraud et al., (1976). An alternative explanation for the depletion of ^{210}Po activity in particles is their lithogenic origin. $^{210}Po/^{210}Pb$ AR in lithogenic particles was reported to be similar to or less than unity (Nozaki et al., 1998; Tateda et al., 2003). In addition, the AR < 1 observed at station 1 (120, 250, and 550 m) could be associated with lithogenic particles from the Iberian Margin where 100% of the particulate Fe (PFe) had a lithogenic origin while the lithogenic contribution to PFe at other stations was smaller (Gourain et al., 2018).

The time-series chlorophyll-a concentrations (8-day composite, https://oceancolor.gsfc.nasa.gov) from January to July 2014 at each station revealed bloom conditions about 4 months prior to the sampling time (Fig. 6). We estimated the days since the last bloom began prior to the sampling date for each station (Table 1) and put these data into the context of the low $^{210}Po_p/^{210}Pb_p$ AR (< 1) in the total particles > 1 μm (Fig. 7). Eight stations had total particulate samples with $^{210}Po_p/^{210}Pb_p$ AR lower than unity from either shallow or deep waters. Specifically, when the time since the last bloom began was relatively short (24 – 47 d) the samples with $^{210}Po_p/^{210}Pb_p$ AR < 1 were observed in the shallow waters (10 – 60 m). In contrast, as longer time (50 – 74 d) passed since the last bloom, the depths at which samples had $^{210}Po_p/^{210}Pb_p$ AR < 1 were found to be much deeper (120 – 500 m). The results indicated that post-bloom particles could be recycled for weeks in shallow depths and take weeks to months to sink to deeper waters.

The averages of $^{210}Po_p/^{210}Pb_p$ AR within the upper 200 m water column were put into a global context with previously reported results (Fig. 8). Total particulate $^{210}Po/^{210}Pb$ AR in the open ocean in previous studies (e.g., Equatorial/western Pacific, Bellingshausen Sea, BATS, Labrador Sea)

were generally greater than unity. In contrast to the open ocean, the data show a distinct trend of depletion of relative ^{210}Po activity in marine particles from the shallow seas of the high latitude northern hemisphere. The lowest total particulate ^{210}Po/^{210}Pb AR values (Table 2, 0.4 – 0.5) were found in the Chukchi shelf (He et al., 2015) and other seas from the Eurasian sector (Barents, Kara and Laptev Seas) but also in central Arctic (Friedrich, 2011). Previous studies have observed depletion of relative ^{210}Po activity in nearshore particles in the Yellow Sea (Hong et al., 1999), in the turbid waters off of western Taiwan (Wei et al., 2012), on the shelf of Woods Hole, MA (Rigaud et al., 2015), and now in the margin station off St. John's, Canada (this study). The previous authors attributed the relative depletion of particulate ^{210}Po activity in the nearshore waters to the terrestrial origin/riverine input of particles with a low ^{210}Po/^{210}Pb AR. This may partially explain low activity ratios in the samples from the shelf of the Arctic Ocean as well, since it receives ~ 10% of global river runoff and is the most riverine-influenced of all of the world's oceans (Opsahl et al., 1999; Carmack et al., 2006). The Arctic Basin, similarly, had widespread deficits of particulate ^{210}Po activity in the upper water column during the sea-ice minimum in 2007 (Roca-Marti et al., in review). Besides shelf particles, the authors suggest that other particle types could also play a role in lowering the particulate AR, including sea-ice sediments, remineralized material, fecal pellets, and picoplankton aggregates.

4.3 Relationship between total particulate ^{210}Po/^{210}Pb AR and AOU

AOU is a time-integrated measure of the amount of oxygen removed during the biogeochemical processes (e.g. respiration, remineralization, oxidation) in the ocean interior. Therefore, AOU is a product of apparent oxygen utilization rate (AOUR) and the age of water mass (e.g. Stanley et al., 2012), i.e. high AOU could be due to either intense biogeochemical processes that have occurred in a short period of time (young water mass) or weaker processes over a longer period of time (old water mass). Consequently, the rate of these biogeochemical processes and time (water mass age) would have different/similar impacts on the $^{210}Po_p/^{210}Pb_p$ AR value depending on the initial AR in the particles and the natural of the particles. For example, the $^{210}Po_p/^{210}Pb_p$ AR would tend to increase with time if the initial AR is < 1 because particulate ^{210}Po activity would increase from the decay of ^{210}Pb and trend towards secular equilibrium ($^{210}Po_p/^{210}Pb_p$ AR = 1), and to decrease with time if the initial AR is > 1 as the original excess of particulate ^{210}Po activity would disappear after 7 half-lives of ^{210}Po. In contrast, oxygen

consumption due to bacterial remineralization would preferentially release ^{210}Po activity from particles into the dissolved pool (e.g. Stewart et al., 2008), leading to a lower $^{210}Po_p/^{210}Pb_p$ AR in those particles.

The combination of average $^{210}Po_p/^{210}Pb_p$ AR and their corresponding average AOU in the upper 200 m at 40 stations from 4 independent studies, including ARK-XXII/2 (77.38 – 87.83 ºN, n = 15) in the Arctic, BOFS (48.89 – 49.87 ºN, n = 7), GA03 (22.38 – 39.70 ºN, n = 7), and GA01 (this study, 40.33 – 59.80 ºN, n = 11) in the North Atlantic (see map in Fig. 8) suggests two distinct linear trends (Fig. 9). When AOU was lower than 25 μmol kg^{-1}, the $^{210}Po_p/^{210}Pb_p$ AR was found to be greater than unity, together with a linear negative relationship (n = 27, R^2 = 0.5, $p < 0.001$) towards the AOU at 25 μmol kg^{-1}. In contrast, AOU values greater than 25 μmol kg^{-1} were coincident with a $^{210}Po_p/^{210}Pb_p$ AR < 1, and there was a linear positive relationship (n = 12, R^2 = 0.4, $p = 0.03$) towards the highest AOU values measured. The two contradictory linear trends likely reflect the nature of the particles. For example, the observation of $^{210}Po_p/^{210}Pb_p$ AR > 1 with AOU < 25 μmol kg^{-1} may suggest relatively fresh/organic particles in the young water mass. When AOU increases either due to water mass aging or higher AOUR, the $^{210}Po_p/^{210}Pb_p$ AR decreases with a slope of -0.17 ± 0.04. On the other hand, refractory/lithogenic particles may be suggested by the observation of $^{210}Po_p/^{210}Pb_p$ AR < 1 with AOU > 25 μmol kg^{-1}. For those particles, increasing in AOU either due to water mass aging or higher AOUR would change the $^{210}Po_p/^{210}Pb_p$ AR to a much lesser degree than that for organic particles with a slope of 0.008 ± 0.003. This explanation, however, appears to only hold for the high latitude Northern Hemisphere where $^{210}Po_p/^{210}Pb_p$ activity ratios were generally lower than those in the other oceanic settings (Fig. 8). In the high latitude Southern Hemisphere near Antarctic (e.g., ANT-X/6), for example, there is no apparent relationship between $^{210}Po_p/^{210}Pb_p$ activity ratios and AOU. This relationship (or lack thereof) deserves more study in the future.

4.4 Relationship among small particles, adsorption, and scavenging

The partitioning coefficient, K_d (L kg^{-1}), has been used to describe the particle adsorption behavior of radionuclides. It is defined as the ratio of the adsorbed radionuclide activity (A_p, dpm 100L^{-1}) to the dissolved radionuclide activity (A_d, dpm 100L^{-1}), normalized by the suspended particulate matter concentration (SPM, μg L^{-1}):

404 $$K_d = \frac{A_p}{A_d} \times \frac{1}{SPM} 10^9 \qquad (1)$$

405 Owing to the different biological and chemical behaviors of ^{210}Po and ^{210}Pb, the interpretation
406 of measured K_d for ^{210}Po (K_d(Po)) may not be as clear as that for ^{210}Pb (K_d(Pb)). As claimed
407 previously in Tang et al., (2017), K_d(Po) is complicated because it appears to reflect both the
408 surface adsorption and potential bioaccumulation.

409 In this study, the size-fractionated data of both radionuclide activity and SPM allowed us to
410 calculate the partitioning coefficients for both radionuclides on small and total particles. The
411 dissolved radionuclide activity was calculated as the difference between total and particulate
412 activity. The coefficients for the small particulate and the total particulate phases were normalized
413 by the SPM in the small and total particulate phases, respectively. We present only the coefficients
414 for the small particulate phases ($K_d(Po)_s$, $K_d(Pb)_s$) and the total particulate phases ($K_d(Po)_p$,
415 $K_d(Pb)_p$) because most of the particulate activity (> 80%) was associated with the small particles
416 along the GEOVIDE transect, and most conceptualized scavenging models consider either the
417 two-box model (dissolved – total particulate phases, i.e. $K_d(Po)_p$) or the three-box model (dissolved
418 – small – large, i.e. $K_d(Po)_s$) (Clegg and Whitfield, 1990; 1991; Rigaud et al., 2015) and thus
419 activity is concentrated from the dissolved phase to the total or small particles.

420 The average values of K_d(Po) was 1.6 times of those of K_d(Pb) in both small and total
421 particulate phases, suggesting a higher affinity with particles for ^{210}Po with respect to ^{210}Pb, which
422 is commonly observed in the global ocean (Bacon et al., 1988; Hong et al., 1999; Masqué et al.,
423 2002; Wei et al., 2014; Tang et al., 2017). The K_d values for the small particulate phase were
424 slightly higher than those for the total particulate phase but overall these values were very similar
425 for both radionuclides (Fig. 10), suggesting that adsorption/scavenging of radionuclides was driven
426 by small particles along the transect. In addition, there are increasing studies which argue that
427 small particles can form aggregates that sink, and their contribution to carbon export could be
428 larger than previously thought (e.g. Richardson and Jackson, 2007; Lomas and Moran, 2011;
429 Amacher et al., 2013; Puigcorbé et al., 2015). We, therefore, recommend combining the activities
430 of both small and large particles into a total particulate fraction in order to explain total ^{210}Po/^{210}Pb
431 disequilibria in the surface waters, and utilizing the characteristics of the total particles (instead of
432 just the large particles) in the estimation of the POC export fluxes (Tang et al., companion paper
433 submitted to this volume).

Traditionally, large particles collected by in-situ filtration with pumps, most commonly defined as particles larger than 53 or 70 μm, were assumed to dominate the sinking flux (Dugdale and Goering, 1967; Bishop et al., 1977; Fowler and Knauer, 1986; Honjo et al., 1992; Walsh and Gardner, 1992) such that the composition (POC/^{210}Po) of the large particle size class was used to convert ^{210}Po fluxes into POC export (e.g. Friedrich and Rutgers van der Loeff, 2002; Cochran and Masqué, 2003; Murray et al., 2005; Stewart et al., 2010; Roca-Martí et al., 2016). Given that the true size spectrum of sinking particles for the timescale relevant to the ^{210}Po/^{210}Pb method is unknown and the POC flux estimates are sensitive to the particulate POC/^{210}Po ratio, both small and large particles should be sampled for POC/^{210}Po due to the variability in the POC/^{210}Po ratio in different size classes (Hayes et al., in review).

5 Conclusions

In this study, we reported the vertical distribution of total and size-fractionated particulate ^{210}Po and ^{210}Pb activities in the North Atlantic during the GEOVIDE GA01 cruise. More than 90% of the radionuclide activity was found in the dissolved phase, while a small proportion was associated with particles in this transect. Total ^{210}Po activity was generally depleted relative to total ^{210}Pb activity in the upper 100 m due to the preferential adsorption of ^{210}Po activity by particles. Such deficiencies of ^{210}Po activities generally extended to the deep waters at most of the stations. In the West European Basin, the excess of ^{210}Po activities at stations 1 and 13 in the North East Atlantic Deep Water was attributed to the release of ^{210}Po during dissolution of sinking biogenic particles.

There appear to be geographic differences in particulate ^{210}Po/^{210}Pb activity ratios measured during GEOVIDE and previous studies, with particularly low values in the high-latitude North Atlantic and Arctic. While this observation deserves more attention, we support previous suggestions that this is due to the terrestrial origin/riverine input of particles with a low ^{210}Po/^{210}Pb AR into the river-dominated shallow seas of the Arctic. The age of the particles and water masses as well as the importance of biogeochemical processes (e.g. respiration, remineralization) may also explain some of these observations, as there was a significant relationship between the total particulate activity ratio and AOU when both were measured in the North Atlantic (> 20 ºN) and Arctic Oceans.

Over 80% of the particulate radionuclide activity was on small particles, indicating that the scavenging of both radionuclides was driven by small particles. Therefore, we suggest considering

the activities of ^{210}Po and ^{210}Pb from both small and large particles in order to study the water column ^{210}Po/^{210}Pb disequilibria and quantify POC export along the GA01 transect. This has been addressed in a companion paper in this issue. We recommend that both small and large particles should be sampled for POC/^{210}Po estimates for the application of the ^{210}Po/^{210}Pb method in future studies of POC export.

Acknowledgements

Thank you to the chief scientists (G. Sarthou and P. Lherminier) of the GEOVIDE cruise, and the captain (G. Ferrand), and crew of the *R/V Pourquoi Pas?* for their support of this work. Many thanks to P. Branellec, F. Desprez de Gésincourt, M. Hamon, C. Kermabon, P. Le Bot, S. Leizour, O. Ménage, F. Pérault, and E. de Saint-Léger for their technical support during the GEOVIDE expedition, and to C. Schmechtig for the GEOVIDE database management. P. Lam is also acknowledged for providing two modified McLane ISP. Special thanks go to the member of the pump group including F. Planchon, V. Sanial, and C. Jeandel. The author would like to thank C. Mariez, S. Roig, F. Planchon, and H. Planquette who helped in providing particle composition data. We also would like to acknowledge the funding agencies: the French National Research Agency (ANR-13-BS06-0014, ANR-12-PDOC-0025-01), the French National Center for Scientific Research (CNRS-LEFE-CYBER), the LabexMER (anr-10-LABX-19), and Ifremer. Funding was provided to P. Masque by the Generalitat de Catalunya (Grant 2017 SGR-1588). This work contributes to the ICTA 'Unit of Excellence' (MinECo, MDM2015-0552). G. Stewart and Y. Tang were supported by NSF award #OCE 1237108. M. Castrillejo and M. Roca-Marti were funded by an FPU PhD studentship (AP-2012-2901 and AP2010-2510, respectively) from the Ministerio de Educación, Cultura y Deporte of Spain. M. Castrillejo was also supported by the ETH Zurich Postdoctoral Fellowship Program (17-2 FEL-30), co-funded by the Marie Curie Actions for People COFUND Program. Additional thanks go to G. Hemming (Queens College) and T. Rasbury (Stony Brook University) for laboratory assistance with the ICP-MS analyses. We also thank two anonymous reviewers for their constructive comments to improve the manuscript.

References:

Amacher, J., Neuer, S. and Lomas, M.: DNA-based molecular fingerprinting of eukaryotic protists and cyanobacteria contributing to sinking particle flux at the Bermuda Atlantic time-series study, Deep Sea Research Part II, 93, 71-83, 2013.

Bacon, M. P.: 210Pb and 210Po results from F.S. "Meteor" cruise 32 in the North Atlantic, PANGAEA, 1977.

Bacon, M. P., Belastock, R. A., Tecotzky, M., Turekian, K. K. and Spencer, D. W.: Lead-210 and polonium-210 in ocean water profiles of the continental shelf and slope south of New England, Continental Shelf Research, 8, 841-853, 1988.

Bacon, M. P., Brewer, P. G., Spencer, D. W., Murray, J. W. and Goddard, J.: Lead-210, polonium-210, manganese and iron in the Cariaco Trench, Deep Sea Research Part A. Oceanographic Research Papers, 27, 119-135, 1980a.

Bacon, M. P., Spencer, D. W. and Brewer, P. G.: 210Pb/226Ra and 210Po/210Pb disequilibria in seawater and suspended particulate matter, Earth and Planetary Science Letters, 32, 277-296, 1976.

Bacon, M. P., Spencer, D. W. and Brewer, P. G.: Lead-210 and Polonium-210 as Marine Geochemical Tracers: Review and Discussion of Results from the Labrador Sea, Natural radiation environment III, T. F. Gesell and W. M. Lowder, 1**,** 473-501, 1980b.

Benetti, M., Reverdin, G., Lique, C., Yashayaev, I., Holliday, N. P., Tynan, E., Torres-Valdes, S., Lherminier, P., Tréguer, P. and Sarthou, G.: Composition of freshwater in the spring of 2014 on the southern Labrador shelf and slope, Journal of Geophysical Research: Oceans, 122, 1102-1121, 2017.

Bishop, J. K. B., Edmond, J. M., Ketten, D. R., Bacon, M. P. and Silker, W. B.: The chemistry, biology, and vertical flux of particulate matter from the upper 400 m of the equatorial Atlantic Ocean, Deep Sea Research, 24, 511-548, 1977.

BODC, Lowry, R. K., Machin, P. and Cramer, R. N.: Compilation of the results of EU-project BOFS, PANGAEA, 2016.

Boyer, T., Conkright, M. E. and Levitus, S.: Seasonal variability of dissolved oxygen, percent oxygen saturation, and apparent oxygen utilization in the Atlantic and Pacific Oceans, Deep Sea Research Part I: Oceanographic Research Papers, 46, 1593-1613, 1999.

Carmack, E., Barber, D., Christensen, J., Macdonald, R., Rudels, B. and Sakshaug, E.: Climate variability and physical forcing of the food webs and the carbon budget on panarctic shelves, Progress in Oceanography, 71, 145-181, 2006.

Ceballos-Romero, E., Le Moigne, F. A. C., Henson, S., Marsay, C. M., Sanders, R. J., García-Tenorio, R. and Villa-Alfageme, M.: Influence of bloom dynamics on Particle Export Efficiency

in the North Atlantic: a comparative study of radioanalytical techniques and sediment traps, Marine Chemistry, 186, 198-210, 2016.

Clegg, S. L. and Whitfield, M.: A generalised model for the scavenging of trace metals in the open ocean: I. Particle cycling, Deep Sea Research Part A. Oceanographic Research Papers, 37, 809-832, 1990.

Clegg, S. L. and Whitfield, M.: A generalied model for the scavenging of trace metals in the open ocean-II. Thorium scavenging, Deep Sea Research Part A. Oceanographic Research Papers, 38, 91-120, 1991.

Cochran, J. K., Bacon, M. P., Krishnaswami, S. and Turekian, K. K.: 210Po and210Pb distributions in the central and eastern Indian Ocean, Earth and Planetary Science Letters, 65, 433-452, 1983.

Cochran, J. K. and Masqué, P.: Short-lived U/Th Series Radionuclides in the Ocean: Tracers for Scavenging Rates, Export Fluxes and Particle Dynamics, Reviews in Mineralogy and Geochemistry, 52, 461-492, 2003.

Cooper, L.: Factors affecting the distribution of silicate in the North Atlantic Ocean and the formation of North Atlantic deep water, Journal of the Marine Biological Association of the United Kingdom, 30, 511-526, 1952.

Coppola, L., Prieur, L., Taupier-Letage, I., Estournel, C., Testor, P., Lefevre, D., Belamari, S., LeReste, S. and Taillandier, V.: Observation of oxygen ventilation into deep waters through targeted deployment of multiple Argo-O2 floats in the north-western Mediterranean Sea in 2013, Journal of Geophysical Research: Oceans, 122, 6325-6341, 2017.

Dugdale, R. C. and Goering, J. J.: uptake of new and regenrated forms of nitrogen in primary production, Limnology and Oceanography, 12, 196-206, 1967.

Duteil, O., Koeve, W., Oschlies, A., Bianchi, D., Galbraith, E., Kriest, I. and Matear, R.: A novel estimate of ocean oxygen utilisation points to a reduced rate of respiration in the ocean interior, Biogeosciences, 10, 7723-7738, 2013.

Fleer, A. P. and Bacon, M. P.: Determination of 210Pb and 210Po in seawater and marine particulate matter, Nuclear Instruments and Methods in Physics Research, 223, 243-249, 1984.

Flynn, W. W.: The determination of low levels of polonium-210 in environmental materials, Analytica Chimica Acta, 43, 221-227, 1968.

Fowler, S. W. and Knauer, G. A.: Role of large particles in the transport of elements and organic compounds through the oceanic water column, Progress in Oceanography, 16, 147-194, 1986.

Friedrich, J.: Polonium-210 and Lead-210 activities measured on 17 water bottle profiles and 50 surface water samples during POLARSTERN cruise ARK-XXII/2, PANGAEA, 2011.

Friedrich, J., Robert, M. and Stimac, I.: Polonium-210 and Lead-210 activities measured on 9 water bottle profiles during POLARSTERN cruise ANT-XXIV/3, PANGAEA, 2011.

Friedrich, J. and Rutgers van der Loeff, M. M.: A two-tracer (210Po–234Th) approach to distinguish organic carbon and biogenic silica export flux in the Antarctic Circumpolar Current, Deep Sea Research Part I: Oceanographic Research Papers, 49, 101-120, 2002.

García-Ibáñez, M. I., Pardo, P. C., Carracedo, L. I., Mercier, H., Lherminier, P., Ríos, A. F. and Pérez, F. F.: Structure, transports and transformations of the water masses in the Atlantic Subpolar Gyre, Progress in Oceanography, 135, 18-36, 2015.

GEOTRACES Planning Group: GEOTRACES Science Plan, Baltimore, Maryland, 2006.

Gourain, A., Planquette, H., Cheize, M., Menzel-Barraqueta, J. L., Boutorh, J., Shelley, R. U., Pereira-Contreira, L., Lemaitre, N., Lacan, F., Lherminier, P. and Sarthou, G.: Particualte trace metals along the GEOVIDE section, Biogeosciences, 2018.

Hayes, C. T., Black, E. E., Andersen, R. A., Baskaran, M., Buesseler, K. O., Charette, M. A., Cheng, H., Cochran, J. K., Edwards, R. L., Fitzgerald, P., Lam, P. J., Lu, Y., Morris, S. O., Ohnemus, D. C., Pavia, F. J., Stewart, G. and Tang, Y.: Flux of particulate elements in the North Atlantic Ocean constrained by multiple radionuclides, Global Biogeochemcal Cycles, in review.

He, J., Yu, W., Lin, W., Men, W. and Chen, L.: Particulate organic carbon export fluxes on Chukchi Shelf, western Arctic Ocean, derived from 210Po/210Pb disequilibrium, Chinese Journal of Oceanology and Limnology, 33, 741-747, 2015.

Heyraud, M., Fowler, S. W., Beasley, T. M. and Cherry, R. D.: Polonium-210 in euphausiids: A detailed study, Marine Biology, 34, 127-136, 1976.

Hong, G.-H., Park, S.-K., Baskaran, M., Kim, S.-H., Chung, C.-S. and Lee, S.-H.: Lead-210 and polonium-210 in the winter well-mixed turbid waters in the mouth of the Yellow Sea, Continental Shelf Research, 19, 1049-1064, 1999.

Honjo, S., Spencer, D. W. and Gardner, W. D.: A sediment trap intercomparison experiment in the Panama Basin, 1979, Deep Sea Research Part A. Oceanographic Research Papers, 39, 333-358, 1992.

Hu, W., Chen, M., Yang, W., Zhang, R., Qiu, Y. and Zheng, M.: Enhanced particle scavenging in deep water of the Aleutian Basin revealed by 210Po- 210Pb disequilibria, Journal of Geophysical Research: Oceans, 119, 3235-3248, 2014.

Ito, T., Follows, M. J. and Boyle, E. A.: Is AOU a good measure of respiration in the oceans?, Geophysical Research Letters, 31, 1-4, 2004.

631 Keeling, R. F., Stephens, B. B., Najjar, R. G., Doney, S. C., Archer, D. and Heimann, M.: Seasonal
632 variations in the atmospheric O2/N2 ratio in relation to the kinetics of air-sea gas exchange, Global
633 Biogeochemical Cycles, 12, 141-163, 1998.
634
635 Kim, G. and Church, T. M.: Seasonal biogeochemical fluxes of 234Th and 210Po in the Upper
636 Sargasso Sea: Influence from atmospheric iron deposition, Global Biogeochemcal Cycles, 15, 651-
637 661, 2001.
638
639 Lam, P. J., Ohnemus, D. C. and Auro, M. E.: Size-fractionated major particle composition and
640 concentrations from the US GEOTRACES North Atlantic Zonal Transect, Deep Sea Research Part
641 II, 116, 303-320, 2015.
642
643 Lomas, M. W. and Moran, S. B.: Evidence for aggregation and export of cyanobacteria and nano-
644 eukaryotes from the Sargasso Sea euphotic zone, Biogeosciences, 8, 203-216, 2011.
645
646 Masqué, P., Sanchez-Cabeza, J. A., Bruach, J. M., Palacios, E. and Canals, M.: Balance and
647 residence times of 210Pb and 210Po in surface waters of the northwestern Mediterranean Sea,
648 Continental Shelf Research, 22, 2127-2146, 2002.
649
650 Menzel-Barraqueta, J.-L., Schlosser, C., Planquette, H., Gourain, A., Cheize, M., Boutorh, J.,
651 Shelley, R., Contreira, L. P., Gledhill, M., Hopwood, M. J., Lherminier, P., Sarthou, G. and
652 Achterberg, E. P.: Aluminium in the North Atlantic Ocean and the Labrador Sea (GEOTRACES
653 GA01 section): roles of continental inputs and biogenic particle removal, Biogeosciences, in
654 review.
655
656 Mercier, H., Lherminier, P., Sarafanov, A., Gaillard, F., Daniault, N., Desbruyeres, D., Falina, A.,
657 Ferron, B., Gourcuff, C., Huck, T. and Thierry, V.: Variability of the meridional overturning
658 circulation at the Greenland–Portugal OVIDE section from 1993 to 2010, Progress In
659 Oceanography, 132, 250-261, 2015.
660
661 Moore, R. M. and Smith, J. N.: Disequilibria between226Ra, 210Pb and 210Po in the Arctic Ocean
662 and the implications for chemical modification of the Pacific water inflow, Earth and Planetary
663 Science Letters, 77, 285-292, 1986.
664
665 Murray, J. W., Paul, B., Dunne, J. P. and Chapin, T.: 234Th, 210Pb, 210Po and stable Pb in the
666 central equatorial Pacific: Tracers for particle cycling, Deep Sea Research Part I: Oceanographic
667 Research Papers, 52, 2109-2139, 2005.
668
669 Nozaki, Y., Dobashi, F., Kato, Y. and Yamamoto, Y.: Distribution of Ra isotopes and the 210Pb
670 and 210Po balance in surface seawaters of the mid Northern Hemisphere, Deep Sea Research Part
671 I: Oceanographic Research Papers, 45, 1263-1284, 1998.
672
673 Nozaki, Y. and Tsunogai, S.: 226Ra, 210Pb and 210Po disequilibria in the Western North Pacific,
674 Earth and Planetary Science Letters, 32, 313-321, 1976.
675

Opsahl, S., Benner, R. and Amon, R. M. W.: Major flux of terrigenous dissolved organic matter through the Arctic Ocean, Limnology and Oceanography, 44, 2017-2023, 1999.

Peck, G. and Smith, J. D.: Uranium decay series radionuclides in the Western Equatorial Pacific Ocean and their use in estimating POC fluxes, J.-M. Fernandez and R. Fichez, Paris, 459-469, 2002.

Puigcorbé, V., Benitez-Nelson, C. R., Masqué, P., Verdeny, E., White, A. E., Popp, B. N., Prahl, F. G. and Lam, P. J.: Small phytoplankton drive high summertime carbon and nutrient export in the Gulf of California and Eastern Tropical North Pacific, Global Biogeochemcal Cycles, 29, 1309-1332, 2015.

Richardson, T. L. and Jackson, G. A.: Small Phytoplankton and Carbon Export from the Surface Ocean, Science, 315, 838-840, 2007.

Rigaud, S., Puigcorbé, V., Camara-Mor, P., Casacuberta, N., Roca-Martí, M., Garcia-Orellana, J., Benitez-Nelson, C. R., Masqué, P. and Church, T.: A methods assessment and recommendations for improving calculations and reducing uncertainties in the determination of 210Po and 210Pb activities in seawater, Limnology and Oceanography Methods, 11, 561-571, 2013.

Rigaud, S., Stewart, G., Baskaran, M., Marsan, D. and Church, T.: 210Po and 210Pb distribution, dissolved-particulate exchange rates, and particulate export along the North Atlantic US GEOTRACES GA03 section, Deep Sea Research Part II, 116, 60-78, 2015.

Roca-Marti, M., Puigcorbe, V., Friedrich, J., Rutgers van der Loeff, M. M., Rabe, B., Korhonen, M., Canara-Mor, P., Garcia-Orellana, J. and Masqué, P.: Distribution of 210Pb and 210Po in the Arctic water column during 2007 sea-ice minimun: particle export in the ice-covered basins, Deep Sea Research I, in review.

Roca-Martí, M., Puigcorbé, V., Rutgers van der Loeff, M. M., Katlein, C., Fernández-Méndez, M., Peeken, I. and Masqué, P.: Carbon export fluxes and export efficiency in the central Arctic during the record sea-ice minimum in 2012: a joint 234Th/238U and 210Po/210Pb study, Journal of Geophysical Research: Oceans, 121, 5030-5049, 2016.

Sarin, M. M., Kim, G. and Church, T. M.: 210Po and 210Pb in the South-equatorial Atlantic:, Deep Sea Research Part II, 46, 907-917, 1999.

Sarin, M. M., Krishnaswami, S., Ramesh, R. and Somayajulu, B. L. K.: 238U decay series nuclides in the northeastern Arabian Sea: Scavenging rates and cycling processes, Continental Shelf Research, 14, 251-265, 1994.

Sarthou, G., Lherminer, P., Achterberg, E. P., Alonso‐Pérez, F., Bucciarelli, E., Boutorh, J., Bouvier, V., Boyle, E. A., Branellec, P., Carracedo, L. I., Casacuberta, N., Castrillejo, M., Cheize, M., Contreira, P. L., Cossa, D., Daniault, N., De Saint‐Léger, E., Dehairs, F., Deng, F., Desprez de Gésincourt, F., Devesa, J., Foliot, L., Fonseca‐Batista, D., Gallinari, M., García‐Ibáñez, M. I., Gourain, A., Grossteffan, E., Hamon, M., Heimbürger, L. E., Henderson, G. M., Jeandel, C.,

722 Kermabon, C., Lacan, F., Le Bot, P., Le Goff, M., Le Roy, E., Lefèbvre, A., Leizour, S., Lemaitre,
723 N., Masqué, P., Ménage, O., Menzel Barraqueta, J. L., Mercier, H., Perault, F., Pérez, F. F.,
724 Planquette, H., Planchon, F., Roukaerts, A., Sanial, V., Sauzède, R., Shelley, R. U., Stewart, G.,
725 Sutton, J., Tang, Y., Tisnérat‐Laborde, N., Tonnard, M., Tréguer, P., van Beek, P., Zurbrick, C.
726 M. and Zunino, P.: Introduction to the French GEOTRACES North Atlantic Transect (GA01):
727 GEOVIDE cruise, Biogeosciences, in review.
728
729 Shelley, R. U., Roca-Martí, M., Castrillejo, M., Sanial, V., Masqué, P., Landing, W. M., van Beek,
730 P., Planquette, H. and Sarthou, G.: Quantification of trace element atmospheric deposition fluxes
731 to the Atlantic Ocean (> 40°N; GEOVIDE, GEOTRACES GA01) during spring 2014, Deep Sea
732 Research Part I: Oceanographic Research Papers, 119, 34-49, 2017.
733
734 Shimmield, G. B., Ritchie, G. D. and Fileman, T. W.: The impact of marginal ice zone processes
735 on the distribution of 210Pb, 210Po and 234Th and implications for new production in the
736 Bellingshausen Sea, Antarctica, Deep Sea Research Part II, 42, 1313-1335, 1995.
737
738 Smetacek, V., de Baar, H. J. W., Bathmann, U., Lochte, K. and Rutgers van der Loeff, M. M.:
739 Export production by 234Th, including 210Po and 210Pb measured on water bottle samples during
740 POLARSTERN cruise ANT-X/6, PANGAEA, 1997.
741
742 Stanley, R. H. R., Doney, S. C., Jenkins, W. J. and Lott, D. E. I.: Apparent oxygen utilization rates
743 calculated from tritium and helium-3 profiles at the Bermuda Atlantic Time-series Study site,
744 Biogeosciences, 9, 1969-1983, 2012.
745
746 Stewart, G., Cochran, J. K., Miquel, J. C., Masqué, P., Szlosek, J., Rodriguez y Baena, A. M.,
747 Fowler, S. W., Gasser, B. and Hirschberg, D. J.: Comparing POC export from 234Th/238U and
748 210Po/210Pb disequilibria with estimates from sediment traps in the northwest Mediterranean,
749 Deep Sea Research Part I: Oceanographic Research Papers, 54, 1549-1570, 2007.
750
751 Stewart, G. M., Bradley Moran, S. and Lomas, M. W.: Seasonal POC fluxes at BATS estimated
752 from 210Po deficits, Deep Sea Research Part I: Oceanographic Research Papers, 57, 113-124,
753 2010.
754
755 Stewart, G. M., Fowler, S. W. and Fisher, N. S.: Chapter 8 The Bioaccumulation of U- and Th-
756 Series Radionuclides in Marine Organisms, Radioactivity in the Environment. Elsevier, Volume
757 13**,** 269-305, 2008.
758
759 Subha Anand, S., Rengarajan, R., Shenoy, D., Gauns, M. and Naqvi, S. W. A.: POC export fluxes
760 in the Arabian Sea and the Bay of Bengal: A simultaneous 234Th/238U and 210Po/210Pb study,
761 Marine Chemistry, 2017.
762
763 Tang, Y., Lemaitre, N., Castrillejo, M., Roca-Marti, M., Masqué, P. and Stewart, G.: The export
764 flux of particulate organic carbon derived from 210Po/210Pb disequilibria along the North Atlantic
765 GEOTRACES GA01 (GEOVIDE) transect, Biogeosciences,
766

Tang, Y., Stewart, G., Lam, P. J., Rigaud, S. and Church, T.: The influence of particle concentration and composition on the fractionation of 210Po and 210Pb along the North Atlantic GEOTRACES transect GA03, Deep Sea Research Part I: Oceanographic Research Papers, 128, 42-54, 2017.

Tateda, Y., Carvalho, F. P., Fowler, S. W. and Miquel, J.-C.: Fractionation of 210Po and 210Pb in coastal waters of the NW Mediterranean continental margin, Continental Shelf Research, 23, 295-316, 2003.

Tonnard, M., Planquette, H., Bowie, A. R., van der Merwe, P., Gallinari, M., de Gesincourt, F. D., Germain, Y., Gourain, A., Benetti, M., Reverdin, G., Treguer, P., Boutorh, J., Cheize, M., Barraqueta, J.-L. M., Pereira-Contreira, L., Shelley, R., Lherminier, P. and Sarthou, G.: Dissolved iron in the North Atlantic Ocean and Labrador Sea along the GEOVIDE section (GEOTRACES section GA01), Biogeosciences, in review.

Towler, P.: Radionuclides measured on water bottle samples during FRANKLIN cruise FR05/92, PANGAEA, 2003.

Towler, P.: Radionuclides measured on water bottle samples during FRANKLIN cruise FR08/93, PANGAEA, 2013.

Verdeny, E., Masqué, P., Maiti, K., Garcia-Orellana, J., Bruach, J. M., Mahaffey, C. and Benitez-Nelson, C. R.: Particle export within cyclonic Hawaiian lee eddies derived from 210Pb–210Po disequilibrium, Deep Sea Research Part II: Topical Studies in Oceanography, 55, 1461-1472, 2008.

Walsh, I. D. and Gardner, W. D.: A comparison of aggregate profiles with sediment trap fluxes, Deep Sea Research Part A. Oceanographic Research Papers, 39, 1817-1834, 1992.

Wei, C., Lin, S., Wen, L. and Sheu, D. D. D.: Geochemical behavior of 210Pb and 210Po in the nearshore waters off western Taiwan, Marine Pollution Bulletin, 64, 214-220, 2012.

Wei, C. L., Yi, M. C., Lin, S. Y., Wen, L. S. and Lee, W. H.: Seasonal distributions and fluxes of 210Pb and 210Po in the northern South China Sea, Biogeosciences, 11, 6813-6826, 2014.

Table 1. Biological characteristics of the water column determined by chlorophyll-a concentration (8-day composite) from Fig. 6, including the date when the last bloom began, the difference in chlorophyll-a concentration between the sampling time and last bloom peak, and the days since the last bloom. Activity ratios of $^{210}Po_p/^{210}Pb_p < 1$ and their corresponding depths are also shown. *NA* indicates that all samples from the corresponding depth range had $^{210}Po_p/^{210}Pb_p$ equal to or greater than 1 (no sample with $^{210}Po_p/^{210}Pb_p < 1$).

Station	Sampling date	The date last bloom began	Last bloom peak-current state	Days since last bloom	$^{210}Po_p/^{210}Pb_p < 1$	
					0-100 m	> 100 m
1	5/19/14	3/6/14	Large	74	*NA*	Yes (120, 250, 500 m)
13	5/24/14	4/7/14	Small	47	Yes (60 m)	*NA*
21	5/31/14	4/7/14	Large	54	*NA*	Yes (120 m)
26	6/4/14	4/15/14	Large	50	*NA*	Yes (400 m)
32	6/7/14	5/9/14	Small	29	*NA*	*NA*
38	6/10/14	5/17/14	Small	24	Yes (60 m)	*NA*
44	6/13/14	5/9/14	Small	35	*NA*	*NA*
60	6/18/14	5/17/14	Large	32	*NA*	*NA*
64	6/19/14	5/17/14	Small	33	Yes (30 m)	*NA*
69	6/22/14	5/25/14	Small	28	Yes (20, 30 m)	*NA*
77	6/26/14	5/25/14	Small	32	Yes (10, 20, 50 m)	*NA*

Table 2. The compilation of total particulate $^{210}Po/^{210}Pb$ activity ratios ($^{210}Po_p/^{210}Pb_p$) averaged in the upper 200 m, including this study.

Region		Sampling Method	Date	Size (μm)	Depth (m)	$^{210}Po_p/^{210}Pb_p$	Reference
Arctic	CESAR	*In-situ* pump	Apr – May 83	> 0.45	2-200	1.2 ± 0.7	(Moore and Smith, 1986)
	Arctic (ARK-XXII/2)	Niskin bottle	Jul-Sep 07	> 1	10-200	0.50 ± 0.20	(Friedrich, 2011)
	Chukchi Shelf	Niskin bottle	Jul-Sep 10	> 0.45	0-90	0.37 ± 0.10	(He et al., 2015)
Atlantic	F.S. Meteor	Niskin bottle	Nov-Dec 73	> 0.4	0-200	3.1 ± 1.4	(Bacon, 1977)
	Cariaco Trench	Niskin bottle	Dec 73	> 0.4	0-200	1.4 ± 0.6	(Bacon et al., 1980a)
	Labrador (R/V Knorr)	Niskin bottle	Jun 75	> 0.4	0-100	3.9 ± 1.5	(Bacon et al., 1980b)
	South of New England	Niskin bottle	Jul 80	> 0.45	4-200	1.8 ± 0.8	(Bacon et al., 1988)
	N. Atlantic (BOFS)	Niskin bottle	May-Jun 89, 90	> 0.45	0-150	6.0 ± 4.5	(BODC et al., 2016)
	South-equa. Atlantic	Niskin bottle	May-Jun 96	> 0.7	10-200	1.3 ± 1.1	(Sarin et al., 1999)
	BATS	Go-Flo bottle	Oct 96	> 0.45	0-200	3.7 ± 3.2	(Kim and Church, 2001)
	N. Atlantic (GA03)	*In-situ* pump	Oct-Nov 10, Nov-Dec 11	> 0.8	30-200	1.5 ± 0.5	(Rigaud et al., 2015)
	N. Atlantic (GA01)	*In-situ* pump	May-Jun 14	> 1	8-200	1.4 ± 0.3	This study
Pacific	North Pacific	Niskin bottle	Nov 73	> 0.4	10-150	8.5 ± 5.7	(Bacon et al., 1976)
	W. Pacific (FR05/92)	Niskin bottle	Jul 92	> 0.45	0-200	1.3 ± 1.0	(Towler, 2003)
	Equa. Pacific	Go-Flo bottle	Aug-Sept 92	> 0.45 or 0.5	0-200	5.1 ± 1.2	(Murray et al., 2005)
	W. Pacific (FR08/93)	Niskin bottle	Nov 93	> 0.45	0-200	16 ± 4	(Towler, 2013)
	W. Pacific (FR07/97)	Niskin bottle	Aug 97	> 0.45	0-200	7.2 ± 1.5	(Peck and Smith, 2002)
	Aleutian Basin	Niskin bottle	Jul-Aug 08	> 0.2	0-200	1.9 ± 3.0	(Hu et al., 2014)
	E. Pacific (GP16)	*In-situ* pump	Oct-Dec 13	> 1	15-200	2.4 ± 0.6	unpublished
Antarctic	S. Ocean (ANT-X/6)	Niskin bottle	Oct-Nov 92	> 0.45	20-200	3.0 ± 1.4	(Smetacek et al., 1997)
	Bellingshausen Sea	Go-Flo bottle	Nov-Dec 92	> 0.45	0-100	14 ± 11	(Shimmield et al., 1995)

	S. Ocean (ANT-XXIV/3)	Niskin bottle	Feb - Apr 08	> 0.45	25-200	1.3 ± 0.9	(Friedrich et al., 2011)
Margin Sea	S. China Sea	Go-Flo bottle	Jan-Oct 07, May 08	> 0.45	0-200	1.7 ± 1.1	(Wei et al., 2014)
	W. Taiwan	Go-Flo bottle	Apr 07	> 0.45	8-25	0.85 ± 0.12	(Wei et al., 2012)
	Yellow Sea	Niskin bottle	Feb 93	> 0.7	0-100	0.88 ± 0.08	(Hong et al., 1999)
	Mediterranean Sea	Sediment trap	Mar-Jun 03		200	4.5 ± 1.0	(Stewart et al., 2007)

815

816

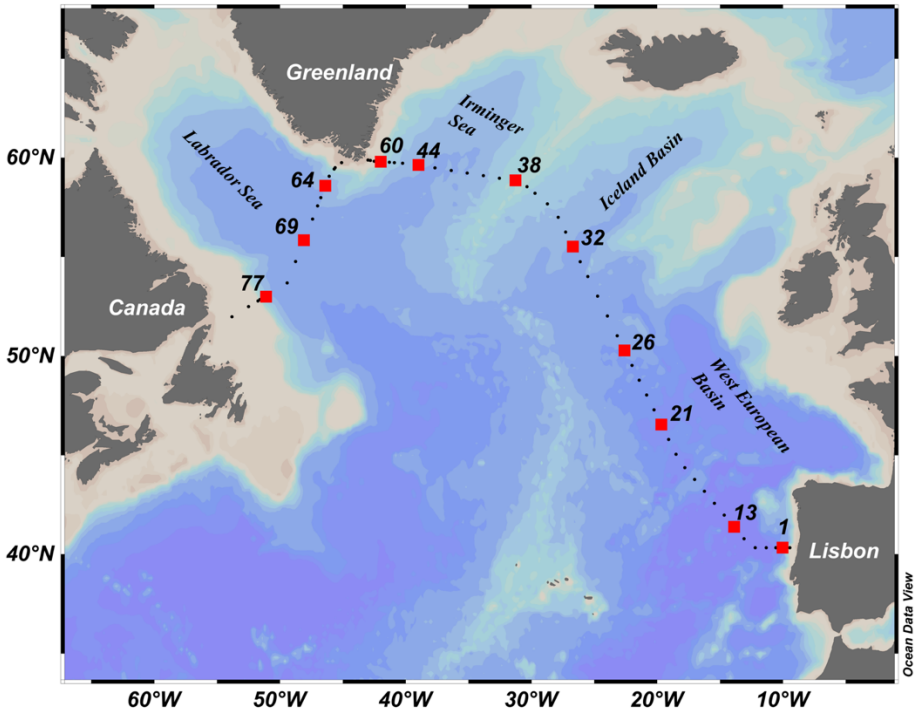

817

818 Fig. 1. Map of the GEOVIDE cruise track (black dots) and the 11 stations sampled for ^{210}Po and
819 ^{210}Pb activity (red squares). Each sampling location is labeled with a station number. The
820 sampling stations are divided into 4 regions (from east to west): West European Basin (stations
821 1, 13, 21, 26), Iceland Basin (stations 32, 38), Irminger Sea (stations 44, 60), and Labrador Sea
822 (stations 64, 69, 77).

823

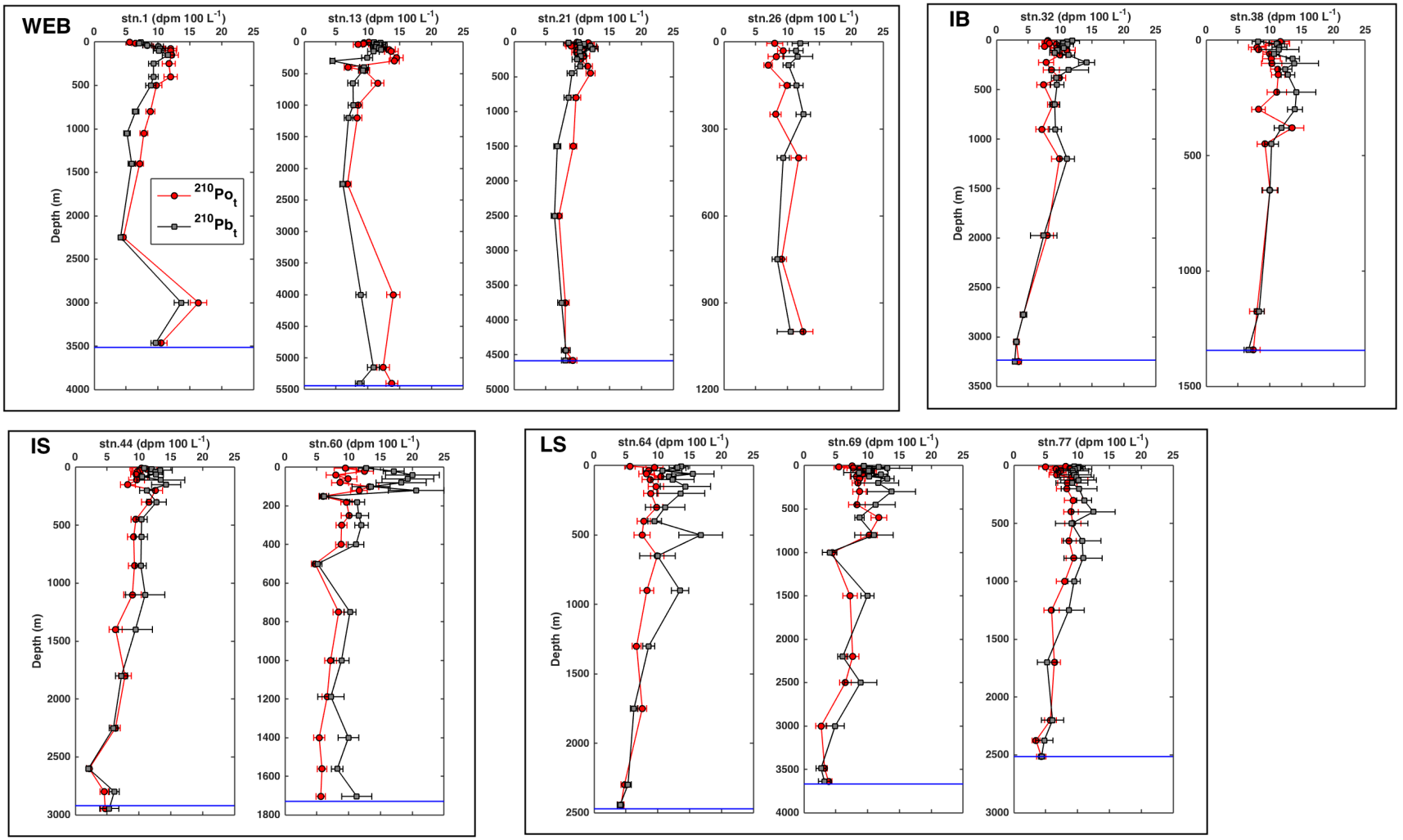

824

825 Fig. 2. The depth profiles of total ^{210}Po ($^{210}Po_t$, red circles) and ^{210}Pb activities ($^{210}Pb_t$, grey squares) along GEOVIDE section. The
826 horizontal blue line is the bottom depth, which coincided with the deepest water sample except for station 26 which was sampled only
827 down to 1000 m. Note that the depth scale for each plot may be different. The profiles are shown in the order of sampling date with

the region indicated on the top left of each box: West European Basin (WEB), Iceland Basin (IB), Irminger Sea (IS), Labrador Sea (LS).

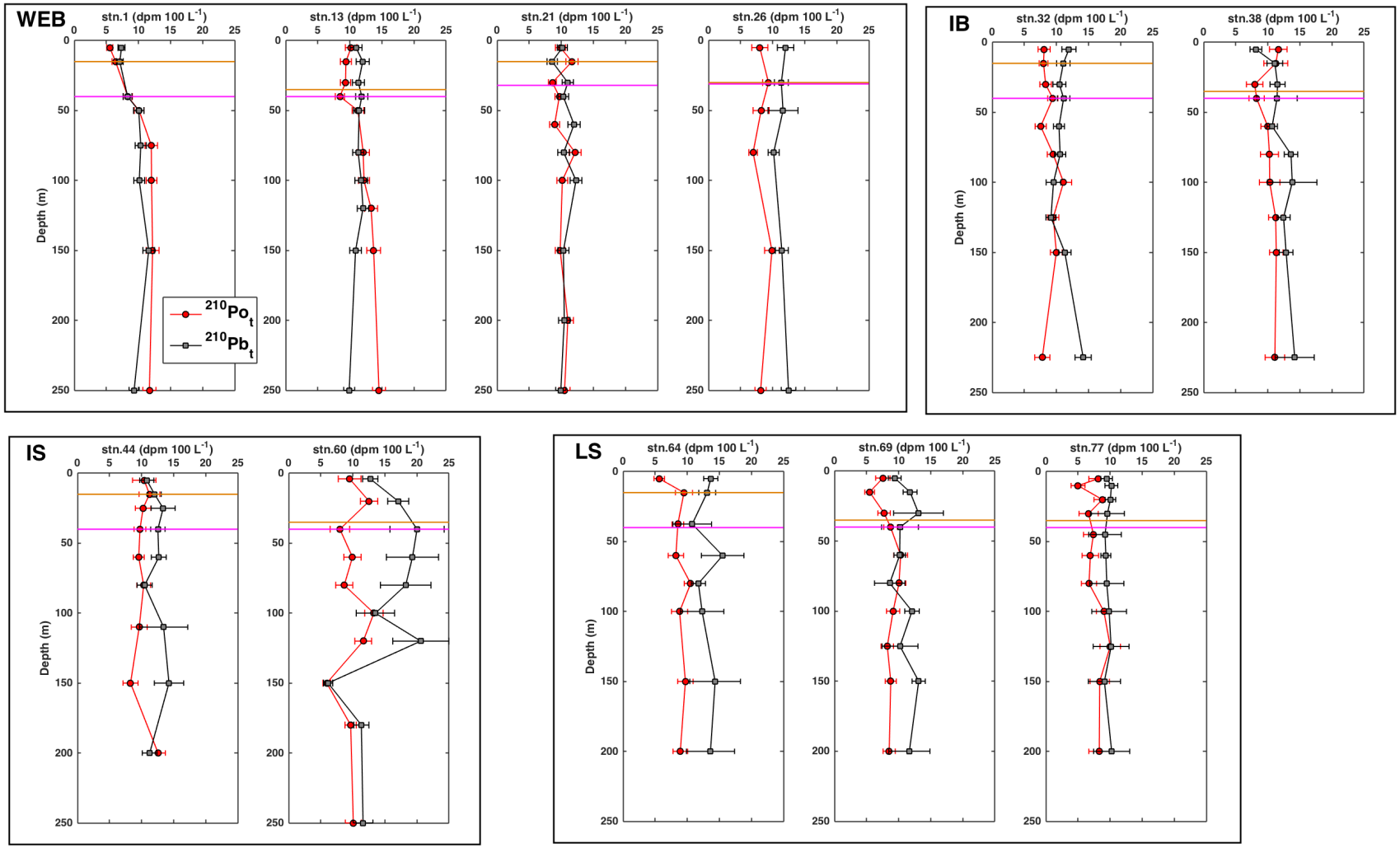

Fig. 3. The upper 250 m of the depth profiles of total ^{210}Po (^{210}Po$_t$, red circles) and ^{210}Pb activities (^{210}Pb$_t$, grey squares) along the GEOVIDE section. The horizontal orange and magenta lines denote the mixed layer depth (MLD) and the base of the euphotic zone

835 ($Z_{1\%}$), respectively. The depth profiles are shown in the order of sampling and grouped by region (refer to Fig. 2 for the text
836 abbreviations).

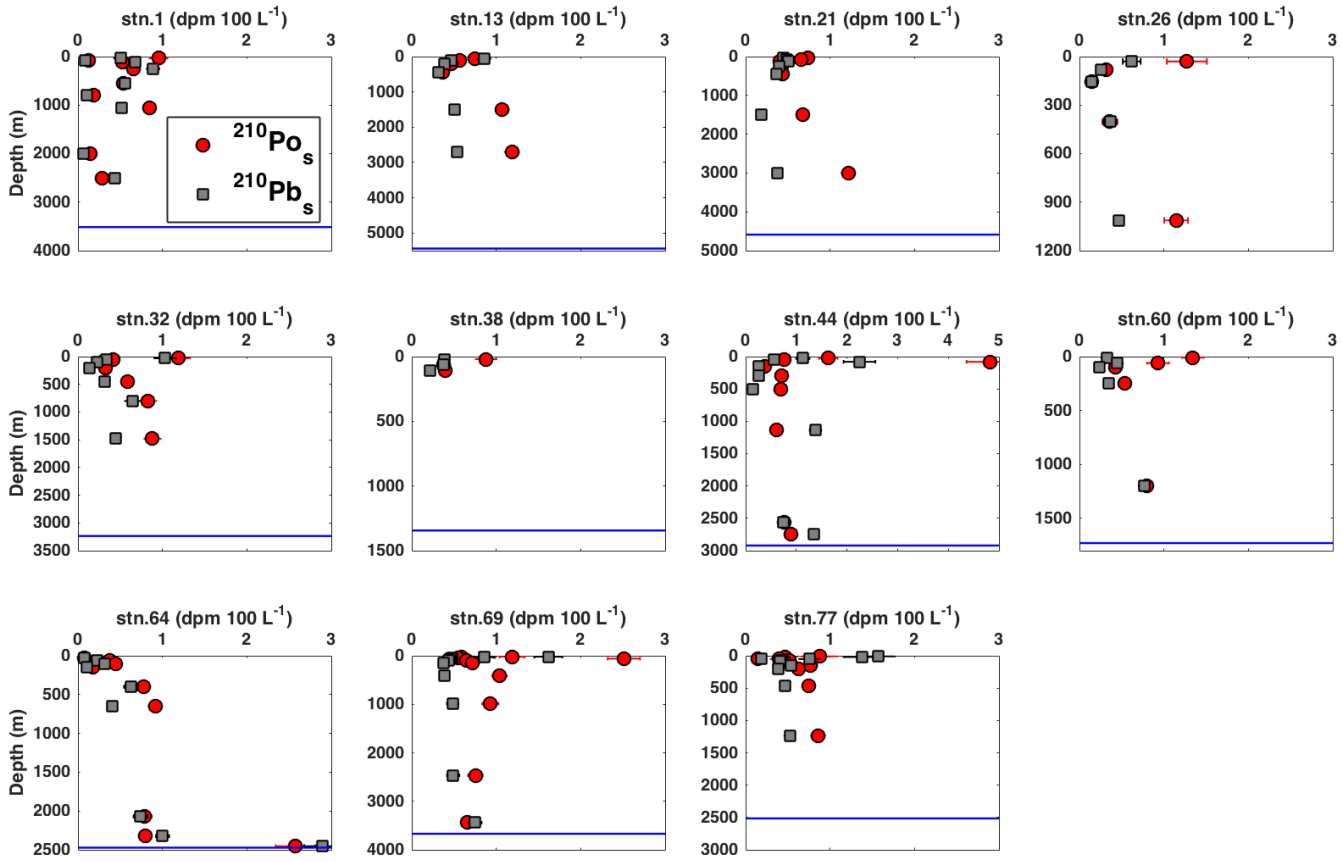

837

838 Fig. 4. Vertical profiles of the particulate ^{210}Po and ^{210}Pb activity in the small size fraction (1-53
839 µm, ^{210}Po$_s$, ^{210}Pb$_s$). Note that the depth scale may differ among plots, and the activity scale at
840 Station 44 differs from the scale on all other plots. The horizontal blue line represents the bottom
841 depth at that station.

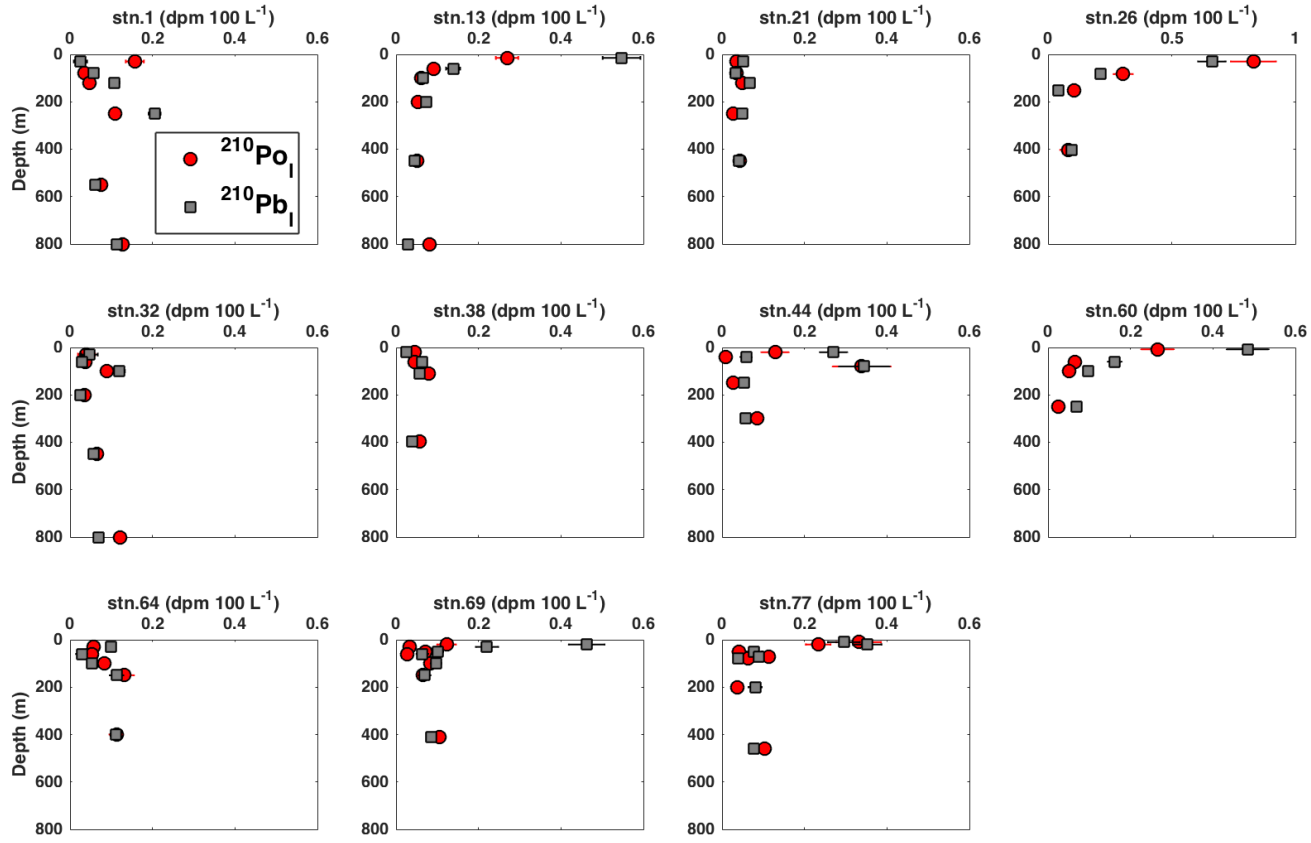

842

843 Fig. 5. The vertical profiles of the particulate ^{210}Po and ^{210}Pb activity in the large size fraction (>
844 53 µm, $^{210}Po_l$, $^{210}Pb_l$) in the top 800 m. Note that the activity scale at Station 26 differs from the
845 scale on all other plots.

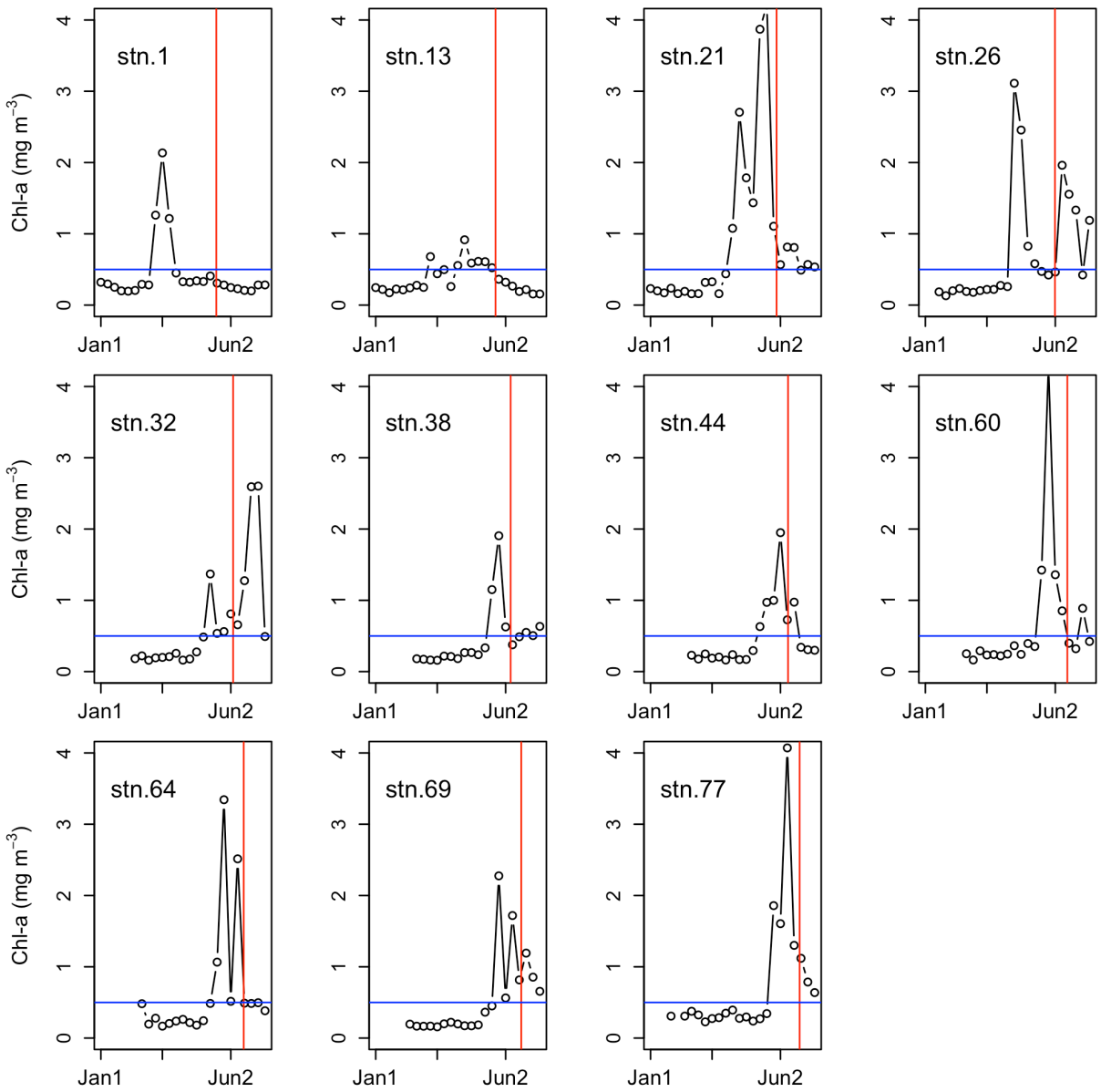

Fig. 6. Time-series (January 1 – July 12, 2014) chlorophyll-a concentrations (8-day averages) from Aqua MODIS (https://oceancolor.gsfc.nasa.gov) at each station along the GA01 transect. The vertical red line denotes the sampling date at each station. The horizontal blue line denotes chlorophyll-a concentration of 0.5 mg m^{-3}. The time when chlorophyll-a concentration first exceeded 0.5 mg m^{-3} after the end of the last bloom defines the date when the next bloom began.

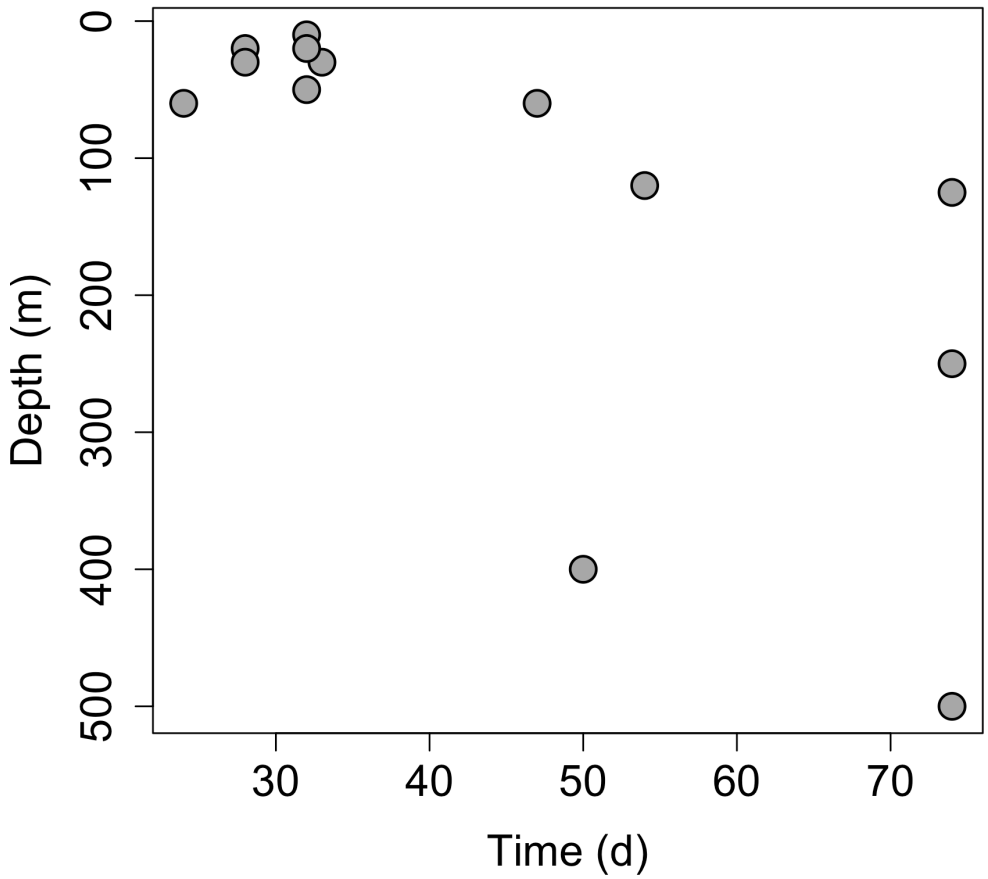

853

854

855 Fig.7. Depths at which the total particulate (> 1 μm) $^{210}Po/^{210}Pb$ activity ratio was lower than
856 unity vs. the time since the last bloom (data is presented in Table 1).

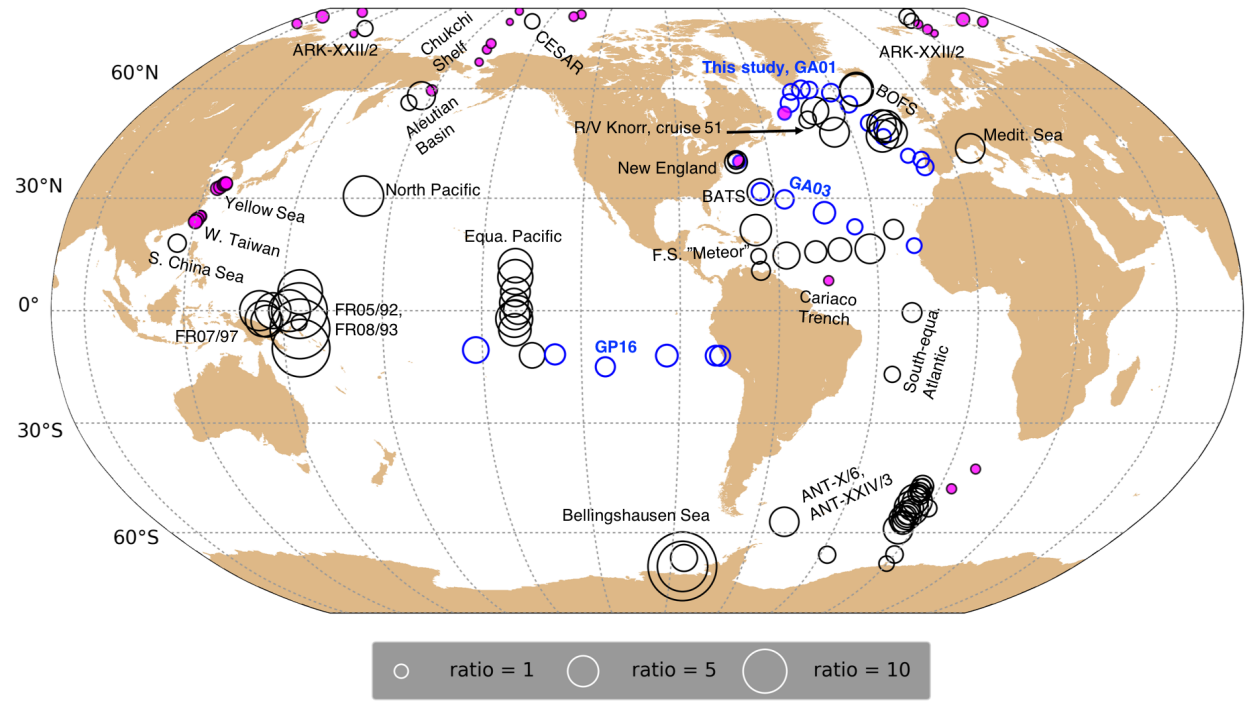

857

858 Fig. 8. Comparison of particulate $^{210}Po/^{210}Pb$ activity ratios in the upper 200 m from this
859 study and 20 previous studies (references in Table 2). Information about the study site,
860 sampling date, method, and particle size of each study are shown in Table 2. The black
861 circles represent data from previous studies while the blue circles are the results from
862 samples analyzed in the Stewart lab from three recent GEOTRACES transects (GA03, GP16,
863 and this study, GA01 GEOVIDE). The filled magenta and open circles indicate activity ratios
864 lower and higher than 1, respectively.

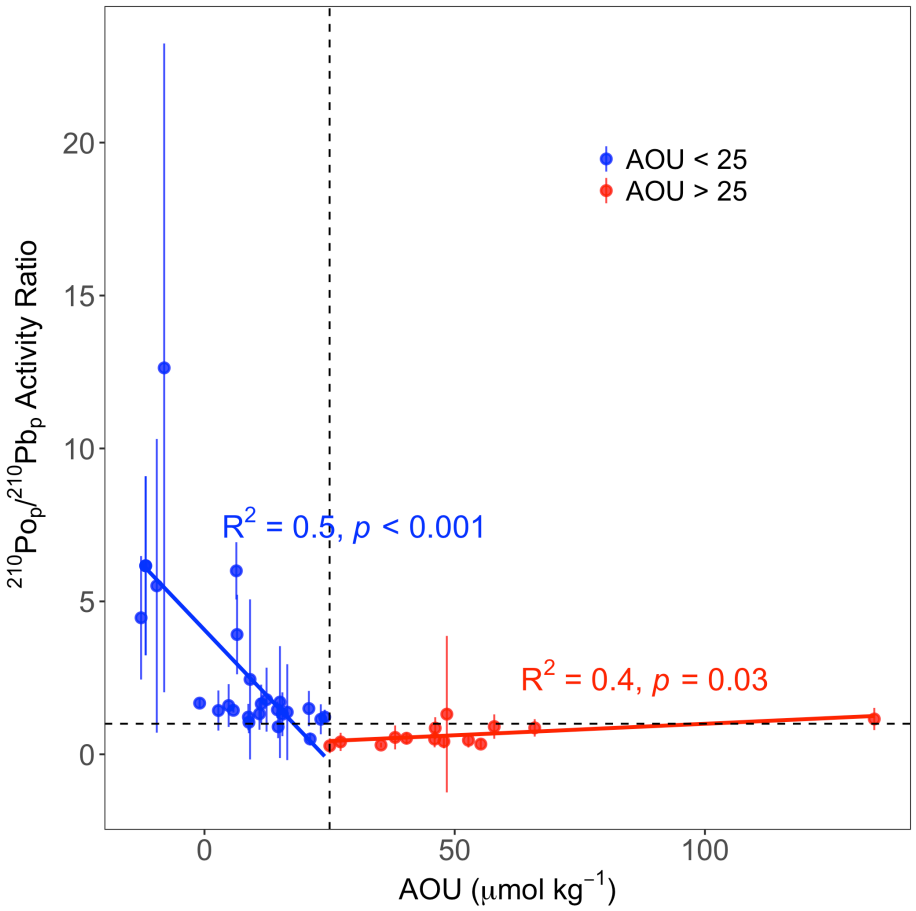

Fig. 9. The relationship between AOU (μmol kg^{-1}) and total particulate ^{210}Po/^{210}Pb activity ratio ($^{210}Po_p/^{210}Pb_p$) from the upper 200 m in the northern hemisphere (> 22 ºN) investigated by a linear regression model (red and blue lines). The 40 stations include data from previous studies, ARK-XXII/2 (77.38-87.83 ºN, n = 15) in the Arctic, BOFS (48.89-49.87 ºN, n = 7), GA03 (22.38-39.70 ºN, n = 7), and this study, GA01 (40.33-59.80 ºN, n = 11) in the North Atlantic. The horizontal dashed line represents $^{210}Po_p/^{210}Pb_p$ AR = 1 and the vertical dashed line represents AOU = 25 μmol kg^{-1}. Blue circles denote AOU < 25 μmol kg^{-1}, while red circles AOU > 25 μmol kg^{-1}.

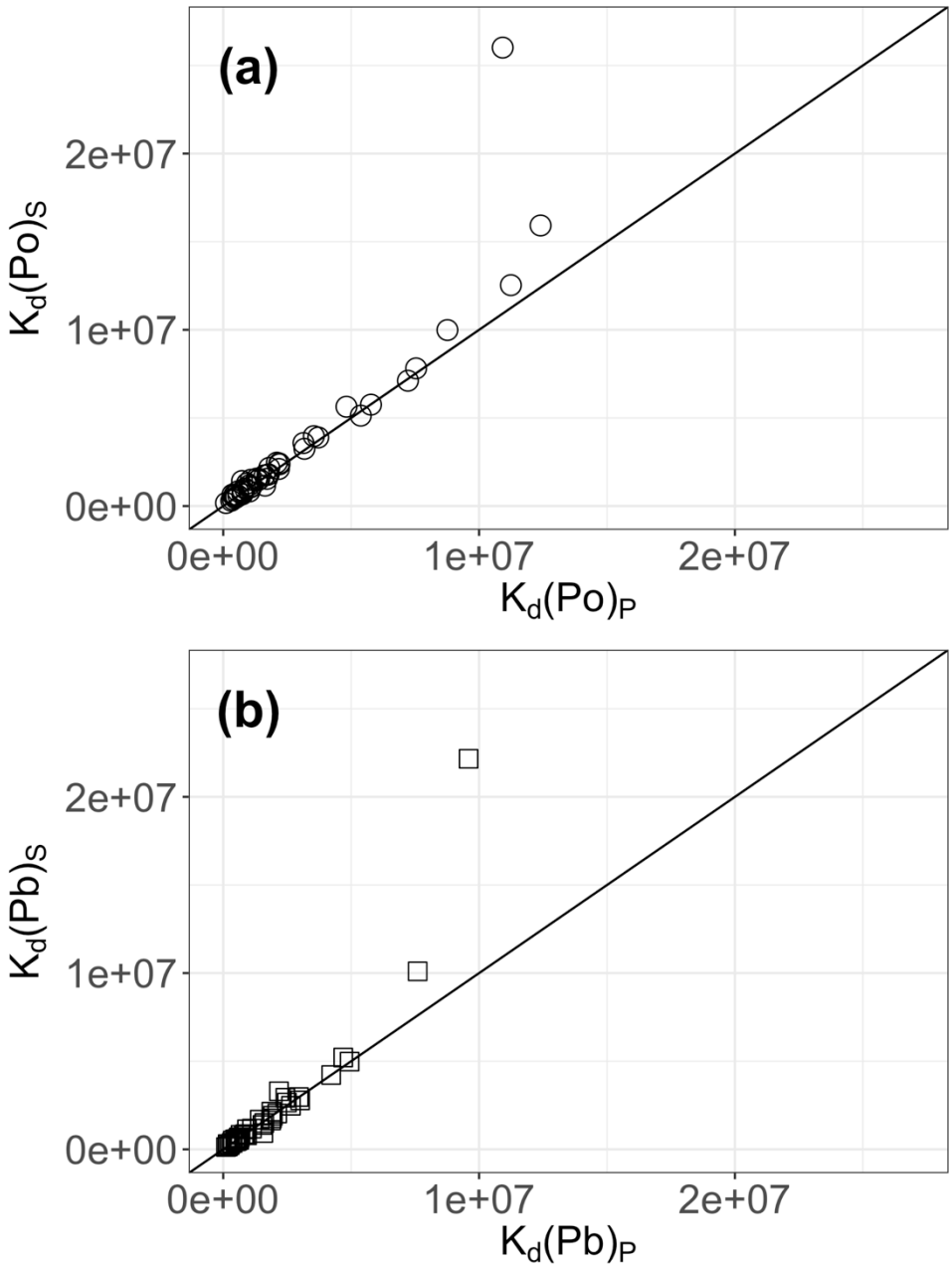

874

875 Fig. 10. Comparison of the partitioning coefficient (K_d) between the dissolved and small
876 particulate phases ($K_d(Po)_s$, $K_d(Pb)_s$) vs. between the dissolved and total particulate phases
877 ($K_d(Po)_p$, $K_d(Pb)_p$) for (a) ^{210}Po and (b) ^{210}Pb. The 1:1 line is indicated as the solid line in
878 each plot.